NASA-TM-112469

Pergamon

Planet. Space Sci., Vol. 44, No. 5, pp. 441–464, 1996
Copyright © 1996 Published by Elsevier Science Ltd
Printed in Great Britain. All rights reserved
0032-0633/96 $15.00+0.00

0032-0633(95)00141-7

NDG
IN-90-TM
032444

On the relationship between transit velocity of interplanetary shocks and solar active processes

Robert M. Wilson

Space Sciences Laboratory, NASA Marshall Space Flight Center, AL 35812, U.S.A.

Received for publication 20 November 1995

Abstract. Recently, it was reported (V. G. Eselevich, *Planet. Space Sci.* **42**(7), 575–582, 1994) that preferential relationships exist between the transit velocity V_T of earthward-directed interplanetary shocks and solar active processes, in particular, eruptive filaments outside active regions (the size of the erupting filament L_f) and solar flares (the value of the X-ray characteristic J). Unfortunately, statistical testing of the proposed associations was not accomplished, nor was the "geoeffectiveness" of the events adequately described. Reported here are the results of a re-examination of the 21 eruptive filaments (SSC-EF events) and 26 X-ray flares (SSC-F events) that have been associated with storm sudden commencements (SSCs) at Earth. Simple statistical testing refutes the claim that a preferential relationship exists between V_T and L_f, while it supports the claim that one exists between V_T and J. More importantly, the inferred relationship between V_T and J is found to be more complicated than previously thought. In particular, it now appears that SSC-F events may be separable into two groups, based on the value of J: a low-J group ($J \leq 56$), in which V_T varies directly with J, and a high-J group ($J > 56$), in which V_T varies inversely with J. As a whole, high-J events are associated with shocks of higher average transit velocity than those of low-J events, and SSC-F events with shocks of higher average transit velocity than those of SSC-EF events. Further, high-J events tend to be of greater X-ray class (>M3), longer duration (>80 min), and are more likely to be associated with type II/IV radio emission (9 of 12) than low-J events. They also tend to occur in magnetically complex (gamma/delta configuration) active regions (10 of 12) that are large in areal extent (area >445 millionths of a solar hemisphere) on the day of flaring (9 of 12). Of the 9 solar proton events that affected the Earth's environment that were found to be associated with SSC-F events, six were high-J events. Concerning "geoeffectiveness", there appears to be no preferential relationship between the value of the J-parameter and the most negative value of the Dst geomagnetic index Dst(min) following the SSC, which is found to usually occur at 6–14 h after SSC onset (18 of 26) and which ranged in value from −1 to −249 (having a median value of about −75). Of the 26 SSC-F events, only 14 can be associated with a Dst(min) ≤ −75, and of these only 7 were high-J events. Of the 14 storm-related events (i.e. Dst(min) ≤ −75), three have previously been identified as being either "magnetic clouds" or "bidirectional flows", both manifestations of earthward-directed coronal mass ejections (CMEs). Superposed epoch analyses of selected solar wind parameters and Dst during the interval of storm-related SSC-F events demonstrate that geoeffective SSC-F events tend to be associated with solar wind flows that are faster, greater in magnetic field strength, and have a rotating field which has a strong southward component shortly after SSC onset, in comparison to SSC-F events that do not have Dst(min) ≤ −75. Therefore, it is inferred that geoeffective SSC-F events are probably fast earthward-directed CMEs. Although no single parameter is found that can serve as a predictor of high-skill level for determining the geoeffectiveness of an SSC-F event prior to its occurrence at Earth, one finds that knowledge of the flare's hemispheric location and appearance or lack of appearance of a two-ribbon structure is sufficient to correctly postdict the geoeffectiveness of 20 out of 25 of the SSC-F events (80%). Surprisingly, the association or lack of association of metric type II/IV radio emission as a characteristc for determining the geoeffectiveness of the SSC-F events proved unfruitful, as did, to a lesser extent, the duration of the X-ray emission.
Copyright © 1996 Published by Elsevier Science Ltd

1. Introduction

Recently, Eselevich (1994) investigated 21 eruptive filaments outside active regions and 26 X-ray flares (with

optical counterparts) that appeared to be well correlated with the occurrences of storm sudden commencements (SSCs) at Earth. In particular, Eselevich compared the inferred transit velocity V_T of the interplanetary shock wave to the size L_f of the eruptive filament for the SSC-eruptive filament associated events (hereafter denoted SSC-EF) and to the value of the so-called J-parameter for the SSC-flare associated events (hereafter denoted SSC-F), where the J-parameter is computed as the product of the maximum intensity I_m (i.e. X-ray class based on 1–8 Å emission) and the square of the time width of X-ray emission τ^2 and is expressed in units of $10^6\,W\,m^{-2}\,h^{-2}$ (cf. Eselevich, 1990). His major findings were that the inferred transit velocity of the shock wave correlates positively both against the size of the filament for the SSC-EF events and against the value of the J-parameter for the SSC-F events. The importance of Eselevich's work is that, provided that the inferred statistical associations are real, one might then be able to better predict the timing of SSC onset at Earth, given either the size of the eruptive filament or the value of the flare's J-parameter (cf. Joselyn, 1995). Unfortunately, Eselevich did not adequately describe the statistical significance of his results by means of simple statistical testing, nor did he address the question of the "geoeffectiveness" of the events as related to the strength of the ensuing geomagnetic storm, if, in fact, any even occurred and, in particular, the relation of these events to manifestations of coronal mass ejections (CMEs) at Earth. The purpose of this study is to address these pertinent issues regarding the Eselevich events.

2. Analysis and results

2.1. *Statistical aspects of the Eselevich events*

Recall that in his analysis of SSC events, Eselevich (1994) considered the time interval August 1978–December 1980 and January 1986–February 1992, as well as a single event date in January 1977 from Cane *et al.* (1986a). According to Eselevich, 153 SSCs were found in the interval. Of these, 47 could be associated with either a particular eruptive filament (21 events) or a particular flare (26 events).

Table 1 lists the 21 eruptive filaments outside active regions studied by Eselevich (1994). In addition to the event date (shown in the second column, under the heading "eruptive filament") which identifies each event by yr–mo–day/UT, the location of the event (third column) in north–south, east–west solar coordinates is given as are the effective distance from Sun center ψ in degrees, the size of the filament L_f in degrees, and the transit velocity V_T for the shock in $km\,s^{-1}$. The circled event numbers denote those events with shock waves at 1 AU coincident with the arrival of the heliospheric current sheet HCS. Of the 21 eruptives, 7 occurred in the northern hemisphere and 14 in the southern hemisphere, and 9 occurred in the eastern hemisphere and 12 in the western hemisphere. Neither distribution of north–south or east–west events displays a statistically significant asymmetry, so that the distributions appear to be the result of chance.

Similarly, Table 2 lists the 26 flares studied by Eselevich (1994). As in Table 1, the event date is given as yr–mo–day/UT (under the heading "Hα flare") and its location in solar coordinates (third column). Also, the Hα flare importance, the computed value of the J-parameter, and V_T, all extracted directly from Eselevich, are given. To the right are ancillary data taken from appropriate issues of SOLAR GEOPHYSICAL DATA (SGD, published by the National Geophysical and Solar-Terrestrial Data Center, NOAA, Boulder, CO 80303, U.S.A.). The ancillary data include, in part, the class (XRC) and duration of the associated X-ray flare in minutes, where the duration is the time from event start to its end (which normally is the time when the X-ray flux level decays to a point halfway between the maximum observed flux and the preflare X-ray background level). They also include the identification of those events that have associated occurrences of metric type II and/or IV radio emission, solar proton events at Earth, and a two-ribbon flare structure. Each proton event is identified by the letter *P* followed by the peak proton flux in proton flux units, where 1 pfu = 1 proton $cm^{-2}\,s^{-1}\,sr^{-1}$ (recall that proton fluxes are integral 5 min averages for energies > 10 MeV at geosynchronous orbit and that the start of a proton event is defined to be the first of three consecutive data points with fluxes > 10 pfu). Two-ribbon flare structure is denoted by the letter *u* (from its flare annotated symbol as used in the SGD). Lastly, the ancillary data include the daily area and magnetic class of the active region from which the flare emanated, where the area *a* is expressed as the corrected area of the sunspot group in millionths of the solar hemisphere and the magnetic class is the Mount Wilson magnetic classification (where *B* denotes beta—a bipolar spot configuration, *BG* beta–gamma—a mixture of polarities in a dominantly bipolar configuration, *D* delta—opposite polarity umbrae within single penumbra, *BD* beta–delta—a beta with a delta configuration, and *BGD* beta–gamma–delta—a beta–gamma with a delta configuration). As before, the circled events denote those events with shock waves at 1 AU coincident with the arrival of the HCS. Of the 26 flares, 19 occurred in the northern hemisphere and 6 in the southern hemisphere with one flare strangely of unknown location (event No. 10). Also, 17 occurred in the eastern hemisphere and 8 in the western hemisphere. Likewise, as before, neither distribution of north–south or east–west events displays a statistically significant asymmetry, so that they can be attributed purely to chance. (Another peculiar event is event No. 16 for which an X-ray flare cannot be located in the SGD, based on the timing information contained in Eselevich (1994).)

Table 3 gives the mean, standard deviation (sd), and sample size (n) for V_T and L_f for various groupings of SSC-EF events and for V_T and J for various groupings of SSC-F events. These values can then be used in hypothesis testing for determining the significance of the differences of the means for selected pair-groupings for the individual parameters shown (V_T, L_f, and J). The various subgroupings include all events; those found at > 35 deg from Sun center ($\Psi > 35$) as compared to those found within 35 deg from Sun center ($\chi \leq 35$), a designation incorporated in Eselevich (1994); coincident (C) and independent (I) events, dependent upon whether or not the shock wave at 1 AU arrives coincidently with the arrival of

Table 1. SSC-eruptive filament associated events (from Eselevich, 1994)*

No.	Eruptive Filament	Loc.	ψ	L_f	V_T
(1)	77-01-26/0243	S40E64	76	35	710
2	78-11-05/0457	S49W15	51	28	390
3	22/1150	N42W18	46	8	620
(4)	79-03-02/1000	S54E03	54	12	490
5	11-27/0621	N06E01	6	16	620
6	80-08-03/0036	S45E14	47	27	650
(7)	16/0531	S13W25	30	18	590
8	17/0318	N36W11	38	13	660
(9)	86-03-03/2220	S14E38	40	15	750
(10)	08-16/0550	N08W36	37	8	450
(11)	87-03-30/1429	N04E19	23	4	430
(12)	88-05-04/0100	S60E22	64	72	890
13	07-18/2430	S31E51	60	26	900
14	10-07/1340	S21W04	26	4	750
(15)	12-15/1600	S06W02	6	12	940
(16)	89-01-01/2100	S29W52	60	12	660
(17)	02/2144	N22W25	33	10	700
18	05-21/1040	S19W10	22	15	930
19	11-24/0907	S27W03	27	12	650
20	91-08-30/0300	N09E21	23	10	1,170
(21)	92-01-21/1100	S03W06	6	10	390

*outside active regions

NOTE: Circled event numbers denote events with shock waves at 1 AU coincident with the arrival of the heliospheric current sheet. ψ is the effective distance from Sun center in degrees; L_f is the size of the filament in degrees; and V_T is the transit velocity in km s^{-1}. Events 1, 2, 5, 7, 8, 9, 10, 11, 12, 16, and 17 are located, respectively, 30, 40, 10, 30, 27, 7, 3, 0, 93, 22, and 18 degrees from a neutral line (according to Eselevich, 1994).

the HCS; north–south and east–west events, to determine whether or not asymmetry exists; and $J > 56$ and $J \leq 56$ events (the basis for this subdivision will become obvious later).

Table 4 gives the results of hypothesis testing (Lapin, 1978, p. 486) for inferring the significance of the difference of the means for the two comparison groups. The basis for this test is the t statistic for independent samples. When the confidence level (cl) is below 90%, a "no" is shown; when $90\% \leq \text{cl} < 95\%$, it is marked "marginally"; and when $\text{cl} \geq 95\%$, a "yes" is shown for the significance. Thus, as an example, when comparing SSC-EF/SSC-F events, one finds that V_T is significantly faster for flares as compared to eruptives. One also finds that eruptives located >35 deg from Sun center tend to have larger L_f than those located ≤ 35 deg. Other noteworthy results are that high-J events ($J > 56$) tend to have larger V_T than low-J events and that independent flare events (FI) tend to have larger V_T than coincident flare events (FC). There appear to be no other statistically significant bases for the

Table 2. SSC-flare associated events

Data From Eselevich (1994)						Ancillary Data From SGD						
No.	Hα Flare	Loc.	IMP	J	V_T	XRC	XR dur.	II/IV	P	u	a	*Mag.*
1	78-09-27/1700	N30W21	2B	28	880	M1	19	—	—	u	180	B
2	10-01/0700	S14E57	2N	40	711	M7	55	II-IV	—	u	150	B
(3)	11-10/0119	N17W01	2B	52	920	M1	7	II-IV	P/38	u	620	BG
(4)	79-03-01/0955	S24E58	3N	12	670	X1	—	II	—	u	60	BG
(5)	06-05/0455	N18E14	3B	355	1,100	X2	103	II-IV	P/950	u	630	BG
6	07-04/1903	N13E35	2B	460	940	M2	63	II	—	—	450	D
7	30/0218	N23E15	3N	36	790	C6	—	II-IV	—	u	140	B
8	80-04-04/1454	N26W36	2N	120	1,110	M5	77	II-IV	—	u	440	BG
9	12-16/0942	N06E24	2B	27	680	M4	65	—	—	—	1,100	BGD
(10)	88-03-04/0100	—	—	14	520	B3	6	—	—	—	—	—
11	08-23/0833	N17E31	3B	53	960	C7	—	—	—	—	10	B
(12)	89-02-26/0323	N42E43	SF	14	480	C6	—	—	—	u	—	—
13	03-06/1354	N33E71	3B	240	920	X15	405	II-IV	P/3,500	—	1,410	BGD
14	14/1646	N32W22	2B	90	1,260	X1	86	—	—	u	3,400	BGD
15	17/1729	N33W61	2B	230	1,360	X6	96	II-IV	P/2,000	—	3,600	BGD
(16)	24/1602	N15W28	SF	37	520	—	—	—	—	—	120	B
17	04-09/0044	N35E29	4B	56	760	X3	78	IV	P/450	u	330	BD
18	11-25/2255	N30E05	2N	300	1,030	X1	54	IV	P/380	u	490	BG
19	12-27/1237	S26W01	SN	280	1,140	M3	150	—	—	—	1,120	BGD
(20)	90-04-08/0344	N24E29	2N	18	480	M1	70	—	—	u	30	B
21	06-10/2139	N09W17	SF	43	740	M1	81	IV	—	—	480	BG
22	08-24/0830	S12E03	1N	144	1,170	M1	152	IV	—	—	990	BD
23	91-05-29/1545	S07E37	1N	175	1,100	M2	118	—	—	—	420	B
24	07-07/0120	N28E00	3B	190	1,320	X1	291	II	P/2,300	u	140	BG
25	10/1207	S22E32	2N	52	1,020	M3	143	II-IV	P/30	—	540	B
(26)	08-25/0026	N23E76	2B	470	760	X2	277	IV	P/240	u	440	B

NOTE: Circled event numbers denote events with shock waves at 1 AU coincident with the arrival of the heliospheric current sheet. J is expressed in units of $10^6 Wm^{-2}h^2$; V_T in km s^{-1}; *XR* dur. in minutes; P in proton flux units; and a in millionths of the solar hemisphere. Events 3, 4, 5, 12, 16, 20, and 26 are located, respectively, 5, 15, 28, 40, 15, 25, and 10 degrees from a neutral line (according to Eselevich, 1994).

Table 3. Means and standard deviations of V_T, L_f, and J for selected groups

Grouping	Subgrouping	Parameter	Mean	sd	n
SSC-EF	All	V_T	682.9	201.4	21
		L_f	17.5	14.9	21
	$\psi > 35$	V_T	651.8	163.7	11
		L_f	29.4	20.2	11
	$\psi \leq 35$	V_T	717.0	240.6	10
		L_f	11.1	4.6	10
	Coincident (C)	V_T	636.4	184.7	11
		L_f	18.9	19.3	11
	Independent (I)	V_T	734.0	216.1	10
		L_f	15.9	8.4	10
	North (N)	V_T	664.3	245.6	7
		L_f	9.9	3.8	7
	South (S)	V_T	692.1	185.2	14
		L_f	21.3	16.9	14
	East (E)	V_T	734.4	227.7	9
		L_f	24.1	20.4	9
	West (W)	V_T	644.2	179.5	12
		L_f	12.5	6.1	12
SSC-F	All	V_T	897.7	258.1	26
		J	136.0	139.5	26
	$J > 56$	V_T	1100.8	172.3	12
		J	254.5	124.4	12
	$J \leq 56$	V_T	723.6	179.6	14
		J	34.4	15.8	14
	Coincident (C)	V_T	681.3	230.4	8
		J	121.5	182.7	8
	Independent (I)	V_T	999.9	210.3	18
		J	142.4	121.3	18
	North (N)	V_T	895.3	263.2	19
		J	148.4	151.8	19
	South (S)	V_T	968.5	221.5	6
		J	117.2	101.8	6
	East (E)	V_T	875.9	236.8	17
		J	155.4	157.3	17
	West (W)	V_T	991.3	279.6	8
		J	110.0	95.4	8

Table 4. Hypothesis testing results of V_T, L_f, and J for selected comparison groups

Parameter	Comparison groups	t statistic	Significant?
V_T	SSC-EF/SSC-F	−3.12	Yes
	$\psi > 35/\psi \leq 35$	−0.73	No
	EFC/EFI	−1.15	No
	EFN/3FS	−0.29	No
	EFE/EFW	1.02	No
	$J > 56/J \leq 56$	5.44	Yes
	FC/FI	−3.47	Yes
	FN/FS	−0.61	No
	FE/FW	−1.07	No
L_f	$\psi > 35/\psi \leq 35$	2.79	Yes
	EFC/EFI	0.45	No
	EFN/EFS	−1.74	Marginally
	EFE/EFW	1.88	Marginally
J	FC/FI	−0.35	No
	FN/FS	0.47	No
	FE/FW	0.75	No

Eselevich events. Hence, there is no reason to suspect hemispheric location for flares or eruptives nor coincidence/independence for eruptives to be discerning factors in correlative analyses involving V_T, L_f, and J.

Table 5 displays the results of linear regression analyses between V_T and L_f, and V_T and J for various groupings of events. Listed are the coefficient of correlation r, the coefficient of determination r^2 (a measure of the amount of variance that the regression can "explain"), the y-axis intercept a, the slope of the regression b, the standard error of the estimate se, the t statistic for the slope, and whether or not the regression is statistically significant (as before in Table 4). The analyses clearly show that none of the inferred regressions of V_T versus L_f for the SSC-EF events is statistically significant, inferring that the best fit is the mean fit. On the other hand, the analyses clearly show that for the SSC-F events, statistically significant regressions can be found for V_T versus J, especially when J is subdivided into high-J ($J > 56$) and low-J ($J \leq 56$) groups.

Table 5. Correlational aspects for selected groupings of events

Association	Grouping	r	r^2	a	b	se	t	Significant?
V_T vs L_f	All	0.22	0.05	630.37	3.00	201.4	0.99	No
	$\psi > 35$	0.36	0.13	566.82	2.89	160.9	1.15	No
	$\psi \leq 35$	0.13	0.02	642.02	6.75	252.6	0.94	No
	EFC	0.55	0.31	536.50	5.28	161.7	2.00	Marginally
	EFI	−0.30	0.09	857.36	−7.76	218.7	−0.89	No
	EFN	0.29	0.08	481.88	18.50	258.1	0.68	No
	EFS	0.25	0.06	634.13	2.73	186.9	0.89	No
	EFE	0.30	0.09	654.81	3.30	232.2	0.82	No
	EFW	−0.26	0.07	740.17	−7.68	181.6	−0.85	No
V_T vs J	All	0.45	0.20	785.36	0.83	235.6	2.46	Yes
	$J > 56$	−0.69	0.47	1342.65	−0.95	131.6	−2.98	Yes
	$J \leq 56$	0.74	0.54	435.69	8.36	126.8	3.76	Yes
	FC	0.62	0.39	585.99	0.78	194.4	1.94	Marginally
	FI	0.42	0.18	890.14	0.73	196.3	1.86	Marginally
	FN	0.38	0.15	796.67	0.66	249.7	1.70	No
	FS	0.79	0.62	767.70	1.71	152.7	2.55	Marginally
	FE	0.42	0.18	776.80	0.64	221.5	1.82	Marginally
	FW	0.70	0.48	767.06	2.04	217.8	2.36	Marginally

Figure 1 displays the scatter plots of V_T versus L_f for the 21 SSC-EF events (top) and of V_T versus J for the 26 SSC-F events (bottom). In both plots the filled symbols identify coincident events and the unfilled symbols independent events. For the SSC-EF events, circles denote events far from Sun center ($\psi > 35$ deg), while triangles denote events closer to Sun center ($\psi \leq 35$ deg). For SSC-F events, circles denote high-J events ($J > 56$), while triangles denote low-J events ($J \leq 56$). This latter subdivision is purely empirical, as the data clearly suggest a behavioral difference between high-J and low-J events, both of which are statistically significant. The vertical and horizontal lines refer to the approximate median values of the distributions. The probability P that the observed distributions, or those more suggestive of a departure from independence (chance), is computed for each sample of events, based on Fisher's exact test for 2×2 contingency tables (Everitt, 1977, p. 12). Thus, the distribution of V_T versus L_f for SSC-EF events could easily have resulted purely from chance. No regression line is drawn for these events because none was found to be statistically significant (recall Table 4). The regression lines are drawn for the SSC-F events, based on the presumed separation of J into two classes.

2.2. *The "geoeffectiveness" of the SSC-flare associated events*

For brevity sake, examination of the "geoeffectiveness" of the Eselevich events will be limited to an examination of the SSC-F events only. From the previous section, it was shown that Eselevich's SSC-F events display strong preferential linear relationships between the transit velocity of the shock and the value of the J-parameter for the associated X-ray flare. Thus, using the value of the J-parameter as a predictor, it is perceived that one can better estimate the transit speed of the associated shock, thus leading to a better determination for the shock's onset time at Earth. While this appears quite useful, it remains to be seen whether or not the SSC-F events typically are "geoeffective" (i.e. associated with increases in geomagnetic activity). This section will address this important issue as it relates to the SSC-F events.

Recall that early studies have shown that SSCs are often associated with large flares and active filaments (e.g. Chao and Lepping, 1974; Cane, 1985; Cane *et al.*, 1986a; Eselevich *et al.*, 1988; Tang *et al.*, 1989). More recently, however, evidence has accumulated linking the SSC (and associated geomagnetic activity) to the passage of CMEs at Earth (e.g. Sheeley *et al.*, 1985; Gosling *et al.*, 1987, 1990, 1991; Wilson, 1987, 1988, 1990; Gosling, 1990; Kahler *et al.*, 1984; Webb and Hundhausen, 1987; Hundhausen, 1988; Harrison and Sime, 1989; Harrison, 1991; Kahler, 1992; Feynman and Hundhausen, 1994). This shift of emphasis from flare/eruptive prominence to CME as the primary driver for transients in the solar wind (and associated geomagnetic activity) has certainly not gone without controversy (e.g. Gosling, 1993, 1995a,b; Cliver, 1995a,b; Hudson *et al.*, 1995; Pudovkin, 1995). Eselevich's SSC-F events (Table 2), thus, may offer insight concerning these matters.

Table 6 identifies the 26 SSC-F events and the value of the daily Ap geomagnetic index for the 7 days following each Hα flare occurrence, where day 0 refers to the date of the Hα flare. The Hα flare occurrence date (yr–mo–da/UT) and the SSC occurrence date (mo–da/h) were taken directly from Eselevich (1994), as was the value of the J-parameter associated with each event. The Ap daily values were taken from appropriate issues of SGD. The asterisk (*) denotes the dates of occurrences of the SSCs relative to the occurrences of the associated Hα flares. Similarly, Table 7 shows the variation of daily Ap value for the 26 SSC-F events relative to SSC occurrence, where day 0 now refers to the date of SSC onset (see Table 6). For completeness sake, the J-values are again reproduced.

Figure 2 (bottom panel) depicts a histogram of SSC onsets relative to the elapsed time (days) from Hα flare

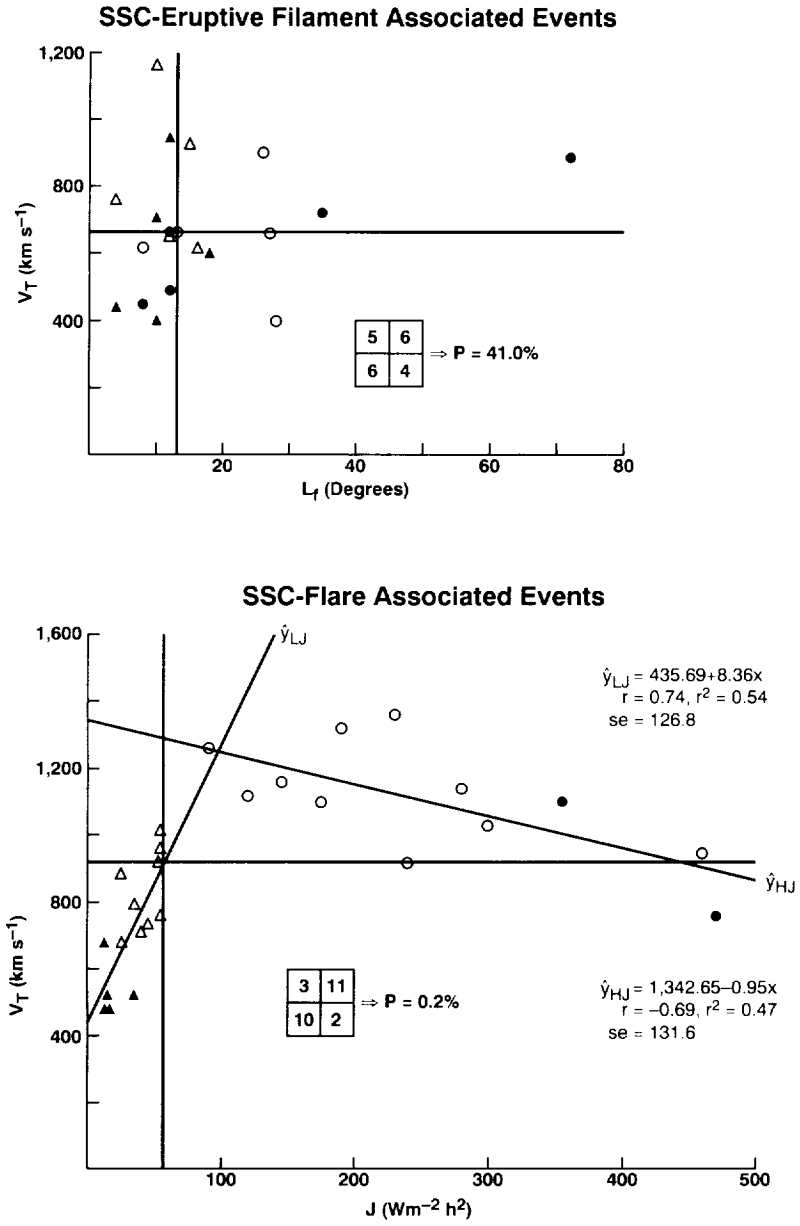

Fig. 1. Scatter plots of shock velocity V_T versus filament size L_f for SSC-EF events (top) and V_T versus J for SSC-F events (bottom). See text for details

occurrence. Clearly, SSCs tend to occur at Earth about 2–3 days following the associated Hα flare (true for 22 out of 26 events). Figure 2 also plots the average daily Ap value (<Ap>) relative to both the Hα flare (upper left panel) and the SSC onset (upper right panel). The average daily Ap value was computed based on the technique of superposed epoch analysis. The vertical bar shown with each average value represents the $\pm$ 1-sigma range for the computed mean value (i.e. $<Ap> \pm s/n^{1/2}$, where n is the number of events in the sample, here equal to 26, and s the sample standard deviation). Again, it is apparent that geomagnetic activity (based on the Ap index) tends to be greater 2–3 days following the Hα flare and on the day of and day following shock onset at Earth. Thus, enhanced geomagnetic activity is construed to be associated with the passage at Earth of SSCs, something realized for sometime (e.g. Akasofu and Chapman, 1972; Patel, 1977).

While geomagnetic activity tends to be greater on the day of and the day following SSC onset, it is apparent (from Tables 6 and 7) that every event did not produce a geomagnetic storm. Recall, that (based on the Ap index) when $Ap \leq 7$, the geomagnetic environment is characterized as "quiet"; when $8 \leq Ap \leq 15$, it is "unsettled"; when $16 \leq Ap \leq 29$, it is "active"; when $30 \leq Ap \leq 49$, it is a "Minor storm"; when $50 \leq Ap \leq 99$, it is a "Major storm"; and when $Ap \geq 100$, it is a "severe storm". Of the 26 SSC-F events, only 17 had $Ap \geq 30$ either on the day of or the day following SSC onset. Thus, for 17 out of the 26 events, the geomagnetic environment was at storm levels either on the day of or the day following SSC onset. From the binomial formula (Lapin, 1978, p. 164), one easily computes the probability of obtaining an $Ap \geq 30$ either on the day of or the day following an SSC onset for ≥ 17 of the 26 SSC-F events to be 8.4%, an interesting

Table 6. SSC-flare associated events and Ap values (relative to Hα flare)

No.	Hα flare	J	SSC	Ap value relative to Hα flare occurrence date (0) 0	1	2	3	4	5	6	7
1	78-09-27/1700	28	09-29/03	51	50	109*	11	13	12	8	17
2	10-01/0700	40	10-04/00	13	12	8	17*	8	4	4	5
3	11-10/0119	52	11-12/03	16	10	53*	22	11	8	6	6
4	79-03-01/0955	12	03-04/05	12	20	13	27*	13	30	7	7
5	06-05/0455	355	06-06/20	4	34*	26	14	15	14	10	7
6	07-04/1903	460	07-06/20	9	9	22*	27	9	6	6	4
7	30/0218	36	08-01/12	9	3	16*	11	10	16	8	18
8	80-04-04/1454	120	04-06/00	11	7	28*	18	17	20	22	30
9	12-16/0942	27	12-19/05	16	5	15	79*	21	26	11	5
10	88-03-04/0100	14	03-07/17	19	8	19	11*	26	13	12	14
11	08-23/0833	53	08-25/08	10	11	15*	9	15	9	13	12
12	89-02-26/0323	14	03-02/03	4	6	13	12	25	37*	13	30
13	03-06/1354	240	03-08/16	24	18	24*	31	19	17	23	246
14	14/1646	90	03-16/05	158	49	50*	34	15	55	14	22
15	17/1729	230	03-19/03	34	15	55*	14	22	39	36	16
16	24/1602	37	03-27/13	16	10	14	44*	39	71	47	52
17	04-09/0044	56	04-11/14	15	8	14*	6	17	24	27	20
18	11-25/2255	300	11-27/20	2	11	16*	28	19	20	38	22
19	12-27/1237	280	12-29/06	25	10	50*	30	35	16	17	15
20	90-04-08/0344	18	04-12/03	6	34	124	64	99*	38	45	24
21	06-10/2139	43	06-13/12	17	11	89	70*	79	9	5	3
22	08-24/0830	144	08-26/06	24	6	63*	15	6	11	26	16
23	91-05-29/1545	175	05-31/10	22	12	52*	74	60	16	58	196
24	07-07/0120	190	07-08/12	7	68*	117	19	20	28	134	75
25	10/1207	52	07-12/09	19	20	28*	134	75	12	22	41
26	08-25/0026	470	08-27/12	10	8	37*	16	14	49	52	47

Note: Asterisk (*) denotes occurrence date for SSC relative to Hα flare. The occurrence dates for SSCs come from Eselevich (1994).

Table 7. SSC-flare associated events and Ap values (relative to SSC)

No.	J	Ap value relative to SSC (0) −1	0	+1	+2
1	28	50	109	11	13
2	40	8	17	8	4
3	52	10	53	22	11
4	12	13	27	13	30
5	355	4	34	26	14
6	460	9	22	27	9
7	36	3	16	11	10
8	120	7	28	18	17
9	27	15	79	21	26
10	14	19	11	26	13
11	53	11	15	9	15
12	14	25	37	13	30
13	240	18	24	31	19
14	90	49	50	34	15
15	230	15	55	14	22
16	37	14	44	39	71
17	56	8	14	6	17
18	300	11	16	28	19
19	280	10	50	30	35
20	18	64	99	38	45
21	43	89	70	79	9
22	144	6	63	15	6
23	175	12	52	74	60
24	190	7	68	117	19
25	52	20	28	134	75
26	470	8	37	16	14

but only marginally significant result. Therefore, just because an SSC occurs, one should not always expect a geomagnetic storm to follow.

Figure 3 compares $Ap \geq 30$ occurrences against the value of the J-parameter for the 26 SSC-F events, based on a 2×2 contingency table analysis (Everitt, 1977, p. 12). Of the 12 high-J valued events ($J > 56$), 9 appear to be associated with geomagnetic storms (events Nos. 5, 13–15, 19, 22–24, and 26); i.e. an $Ap \geq 30$ either on the day of or the day following SSC onset at Earth. The probability P of obtaining ≥ 9 associations can easily be computed (from the binomial formula) to be 7.3%, again, an interesting, but only marginally significant statistical result. Perhaps, one should have expected, at least, some semblance of a possible association, since by their very nature, high-J values imply large flares of especially long duration (recall the definition of J), which, in turn, often have been associated with mass motion, CMEs, and the generation of interplanetary shocks (e.g. Nonnast *et al.*, 1982; Cane *et al.*, 1986b; Kahler *et al.*, 1989; Webb *et al.*, 1994). While a possibly meaningful association may exist between high-J valued flares and the occurrence of enhanced geomagnetic activity, for the 14 low-J valued flares ($J \leq 56$), no such preferential association is inferred. Low-J valued events are essentially equally likely to be associated, or not associated, with geomagnetic storm conditions. Likewise, of the 9 events which did not have associated with them an $Ap \geq 30$, 6 were of low-J value (events Nos. 2, 4, 7, 10, 11, and 17), and of the 17 which could possibly be associated with $Ap \geq 30$, 8 were of low-J value (events

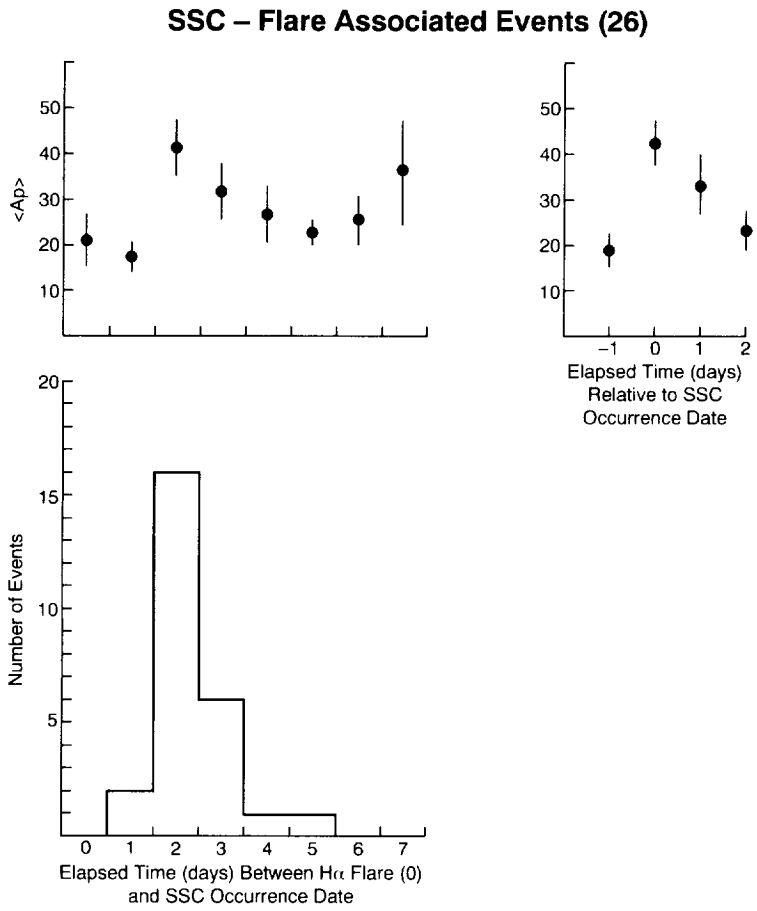

Fig. 2. Geomagnetic activity for SSC-F events. See text for details

Nos. 1, 3, 9, 12, 16, 20, 21, and 25). Thus, taken together, there appears to be no real statistically significant preferential relationship between the occurrence of storm conditions at Earth (i.e. $Ap \geq 30$) and the J-value for the associated flare. The probability of obtaining the observed distribution, or one more suggestive of a departure from independence (chance), is computed to be $P = 29.6\%$. Hence, high J-value alone should not be perceived to be indicative of a flare that will be "geoeffective", a finding supporting the contention of Eselevich *et al.* (1988).

An alternate index to the Ap index is the Dst geomagnetic index, related to the equatorial ring current in the Earth's magnetosphere and useful for identifying geomagnetic storms (Wilson, 1987, 1990). Table 8 tabulates the 26 SSC-F events, identifying the value of the J-parameter (for completeness), the maximum daily Ap value, Ap(max), registered either on the day of SSC onset (denoted 0) or the following day (denoted 1), and the minimum hourly Dst value, Dst(min), during the 24 h interval following SSC onset, where the number of hours elapsed since SSC onset is identified in parentheses. The minimum Dst is defined here as the largest negative excursion in the Dst index during the interval of consideration. A comments column is included which notes the five events that had a slightly more negative Dst(min) value at a later time (i.e. within a 36 h interval following SSC onset). The Dst(min) values were taken from appropriate issues of SGD.

		Ap ≥ 30*	
		No	Yes
J > 56	Yes	3	9
	No	6	8

⇒ P = 29.6%

NOTE: Asterisk (*) means on SSC – occurrence date (0) or the following day (+1).

Fig. 3. 2 × 2 contingency table analysis of Ap and J for the SSC-F events. See text for details

Figure 4 displays the scatter plot of Dst(min) versus Ap(max). The vertical and horizontal lines represent the median values of the two parameters. A 2 × 2 contingency table analysis suggests that the two parameters are strongly related, in that, the probability of obtaining the observed distribution, or one more suggestive of a departure from independence, is computed to be $P = 0.002\%$. Thus, high values of Ap(max) (i.e. $Ap(max) \geq 40$) tend to associate with large negative Dst(min) (i.e. $Dst(min) \leq -75$) and, conversely, low values of Ap(max) tend to associate with small negative Dst(min). The five events that had later occurring more negative Dst(min)

Table 8. CF3SSC-flare associated events with corresponding Ap(max) and Dst(min) values

No.	J	Ap(max) [0,1]	Dst(min) [0–24]	Comments
1	28	109(0)	−241(8)	
2	40	17(0)	−69(12)	
3	52	53(0)	−107(10)	
4	12	27(0)	−69(7)	
5	355	34(0)	−38(11)	
6	460	27(1)	−31(20)	
7	36	16(0)	−1(18)	
8	120	28(0)	−22(18)	−23(26)
9	27	79(0)	−249(14)	
10	14	26(1)	−57(14)	
11	53	15(0)	−19(12)	
12	14	37(0)	−59(8)	−68(30)
13	240	31(1)	−103(10)	
14	90	50(0)	−118(9)	−120(31)
15	230	55(0)	−110(13)	
16	37	44(0)	−92(11)	
17	56	14(0)	−17(0)	
18	300	28(1)	−44(8)	
19	280	50(0)	−172(6)	
20	18	99(0)	−103(19)	
21	43	79(1)	−96(0)	
22	144	63(0)	−116(8)	
23	175	74(1)	−81(7)	
24	190	117(1)	−172(24)	−198(27)
25	52	134(1)	−55(22)	−185(31)
26	470	37(0)	−60(11)	

values are shown as "boxes". Linear regression analysis using the observed Dst(min) [0–24] hour values results in the solid line identified as $\hat{y}$. The correlation coefficient (r) measures −0.68 and the standard error of estimate (se) 47.5. About 46% of the variance in Dst(min) can be explained by the regression. If, instead, one uses the Dst(min)[0–36] hour values, linear regression analysis results in the dashed line y'. It has a correlation coefficent of −0.86 and a standard error of estimate of 34.8. Now, the inferred regression can explain about 74% of the variance in Dst(min). The importance of Fig. 4 is that, clearly, Dst(min) is related to Ap(max). Therefore, one is justified in using the hourly values of Dst to examine more closely the timing aspects of geomagnetic behavior relative to SSC onset.

Figure 5 compares occurrences of Dst(min) ≤ -75 against occurrences of $J > 56$ for the 26 SSC-F events by means of a 2×2 contingency table analysis. As before (Fig. 3), no evidence is found to suggest a preferential association between the occurrence of enhanced geomagnetic activity and the value of the J-parameter. The probability of obtaining the observed distribution, or one more suggestive of a departure from independence, is computed to be $P = 48.8\%$. Some subtle differences are noted between the displayed distributions of Figs 3 and 5. Namely, events Nos. 5, 12, and 26 which appeared as events associated with high geomagnetic activity (based on Ap(max)) in Fig. 3, now appear as events of low geomagnetic activity (based on Dst(min)) in Fig. 5.

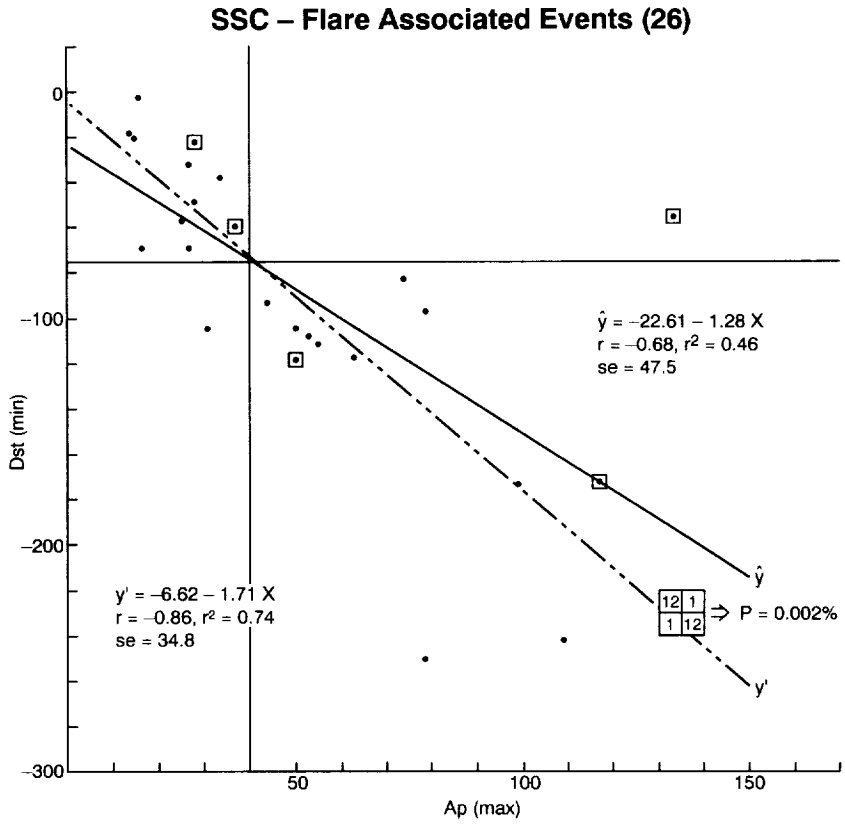

Fig. 4. Dst(min) versus Ap(max) for the SSC-F events. See text for details

J > 56	Dst (min) ≤−75* No	Dst (min) ≤−75* Yes
Yes	5	7
No	7	7

⇒ P = 48.8%

NOTE: Asterisk (*) means in the interval 0–36 h following SSC onset at Earth.

Fig. 5. 2 × 2 contingency table analysis of Dst(min) and *J* for the SSC-F events. See text for details

Figure 6 shows the frequency distribution (histogram) of the occurrences of Dst(min) relative to the corresponding SSC onset, in hours, where elapsed time 0 denotes SSC onset. Clearly, the geomagnetic response to the SSC-F events is delayed until several or more hours following SSC onset. Eighteen of the 26 events have Dst(min) at elapsed time 6–14 h following SSC onset. Only two events (Nos. 17 and 21) have their Dst(min) concurrent with SSC onset. The delayed geomagnetic response for the SSC-F events is reminiscent of the observed behavior associated with the passage of "magnetic clouds" and "bidirectional solar wind flows" (Wilson, 1987, 1988, 1990; Marsden *et al.*, 1987; Gosling *et al.*, 1990, 1991; Gosling, 1990; Richardson, 1994), perhaps, suggesting that the primary driver for the transient geomagnetic activity is a fast earthward-directed CME.

Table 9 compares the values of the *J*-parameter (again for completeness), the Dst(min)[0–36], and solar wind plasma (velocity, density, and temperature) and field (magnetic field strength $|B|$ and B_z direction) extremes during the interval 0–36 h following SSC onset. The solar wind plasma and field measures were taken from Couzens and King (1986), King (1989), and King and Papitashvili (1994). Extreme values are available for all events except Nos. 8 (temperature) and 25 (magnetic field strength and B_z direction).

Figure 7 depicts the scatter plots of Dst(min) against each of the plasma and field parametric extremes tabulated in Table 9. Given for each scatter plot is the result of a 2 × 2 contingency table analysis, and for all the parameters except density (denoted "Den") the result of a linear regression analysis is also shown.

On the association of Dst(min) and solar wind velocity (denoted "Vel"), one finds that large negative Dst(min) (i.e. Dst(min) ≤ -75) tends to be associated with high velocity solar wind (vel $\geq 660\,\mathrm{km\,s^{-1}}$), while small negative Dst(min) tends to be associated with lower solar wind speed. For Eselevich's SSC-F events, the solar wind speed always exceeded $400\,\mathrm{km\,s^{-1}}$. The regression line shown for Dst(min) versus Vel excludes event No. 9 (the circled event). Event No. 9 has the distinction of having the largest negative excursion in Dst, yet is not associated with a particularly fast solar wind flow. More will be spoken of this event (and other peculiar events, see below) later (Section 3.2).

Concerning solar wind density (denoted "Den"), there appears to be no statistically significant relationship between the level of geomagnetic activity and the density of the solar wind. Similarly, for solar wind temperature (denoted "Temp/1000"), it too does not provide a useful measure for gauging the level of geomagnetic activity. Excluding events Nos. 9 (the circled event) and 22 (the boxed event), one deduces a subtle relationship between Dst(min) and temperature, one that is of comparable strength to that based on velocity. Events Nos. 9 and 22 had the lowest and highest temperature extremes, respectively, of the SSC-F events.

Concerning the magnetic field strength of the solar wind (denoted $|B|$), one finds that large negative Dst(min) tends to be associated with events of high $|B|$ (i.e. $|B| \geq 23$ gammas or nT), while small negative Dst(min) tends to be associated with events of low $|B|$. For Eselevich's SSC-F events, the magnetic field strength always had a peak value in excess of 10 gammas. Excluding event No. 5 (the triangle), one finds a regression that is of comparable strength to that of velocity or temperature. Event No. 5 had the greatest magnetic field strength of the SSC-F events.

The lone parameter that seems to characterize Dst(min) better than any other is the north–south directional component of the interplanetary magnetic field (denoted "B_z"). Large negative Dst(min) appears to be strongly associated with strong southward B_z ($B_z \leq -9$), while small negative Dst(min) is associated with weak southward B_z. Thus, when the solar wind flow behind the SSC for Eselevich's SSC-F events has a strong southward com-

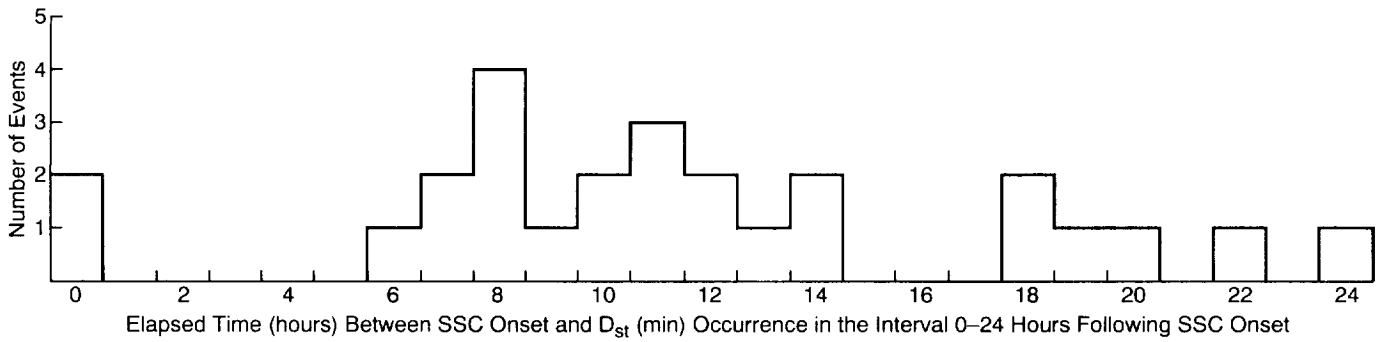

Fig. 6. Histogram of Dst(min) occurrences relative to SSC onsets for the SSC-F events

Table 9. SSC-flare associated events with corresponding extreme values for solar wind plasma parameters and magnetic field parameters for interval 0–36 h

No.	J	Dst(min) [0–36]	Vel	Den	Temp/1000	$\|B\|$	B_z
1	28	–241	912	11.0	1389	28.9	–24.4
2	40	–69	464	18.0	201	11.8	–5.7
3	52	–107	663	34.7	911	29.0	–12.6
4	12	–69	467	22.2	264	15.8	–12.1
5	355	–38	647	38.9	893	54.4	–7.7
6	460	–31	648	16.8	460	14.3	–10.2
7	36	–1	559	7.9	178	10.7	–4.7
8	120	–23	658	8.3	—	11.2	–5.9
9	27	–249	570	52.9	164	35.5	–31.1
10	14	–57	511	59.4	242	16.2	–5.4
11	53	–19	700	12.6	546	18.4	0.0
12	14	–68	618	18.7	382	15.0	–7.8
13	240	–103	551	23.8	446	17.6	–9.3
14	90	–120	743	12.5	375	23.7	–8.1
15	230	–110	880	9.7	503	22.7	–7.6
16	37	–92	501	67.8	433	16.1	–5.7
17	56	–17	440	41.2	279	21.5	–1.7
18	300	–44	739	22.2	906	29.8	–5.0
19	280	–103	740	16.3	745	18.4	–12.0
20	18	–172	757	84.6	714	33.1	–14.5
21	43	–96	732	43.2	430	24.2	–14.7
22	144	–116	785	24.0	2119	22.6	–12.6
23	175	–81	665	33.5	396	20.0	–10.8
24	190	–198	747	13.5	807	32.5	–24.5
25	52	–185	682	19.5	628	—	—
26	470	–60	468	34.5	618	27.7	–16.5

ponent, one finds that the level of geomagnetic activity tends to be enhanced; conversely, when the solar wind flow behind the SSC has a weak southward component, one finds that the level of geomagnetic activity tends to be subdued. The inferred regression has a correlation coefficient of 0.87 and a standard error of estimate of 33.6, and the regression can explain about 75% of the variance in Dst(min).

Because past research has indicated that the level of geomagnetic activity stimulated by Earth passage of a shock disturbance or CME is related directly to the magnitude of the flow speed, magnetic field strength, and southward field component (Gosling *et al.*, 1991), it might be that a bivariate analysis (e.g. Ehrenberg, 1982, p. 200) employing both Vel and B_z might yield a regression that fits Dst(min) better than the one of just using B_z alone. Such an analysis (not shown) results in the regression $\hat{y} = 58.97 - 0.11x_1 + 7.32x_2$, where $\hat{y}$ represents the inferred Dst(min), x_1 the observed Vel, and x_2 the observed B_z. Although the bivariate regression has a slightly higher coefficient of correlation ($r = 0.89$) and smaller standard error (se = 30.8) than the simple linear fit (based on B_z), a comparison of residuals (observed value minus inferred value) shows that 15 of 25 events are better fit using the simple linear regression fit rather than the more complicated bivariate fit. So, while velocity may very well be an important parameter regarding the level of geomagnetic activity, for Eselevich's SSC-F events the main determinator as to "geoeffectiveness" appears to be the strength of the southward component of the interplanetary magnetic field.

3. Discussion

3.1. *Statistical aspects*

Concerning the statistical aspects of Eselevich's events, recall that Eselevich (1994) has reported that V_T is preferentially associated with L_f for eruptive filaments outside active regions (the SSC-EF events), stating that the shock velocity decreases with increasing distance of the filament from the center of the Sun. The results of the present investigation refute this claim. From Table 5, recall that for the all-inclusive grouping of SSC-EF events, the association between V_T and L_f is not statistically significant. Only if one reduces the sample to purely coincident events does one achieve a result that is only of marginal statistical significance (i.e. cl $\geq$ 90%) (cf. Mendoza and Perez-Enriquez, 1993, 1995). If instead of comparing V_T against L_f, one compares V_T directly against ψ (the distance in degrees from Sun center), the same result occurs; namely, the association between V_T and ψ is not statistically significant, whether one uses all events or limits oneself to coincident events. Likewise, if one compares V_T against L_f, subdividing the SSC-EF events into coincident and independent events and further subdividing these into events closer to Sun center ($\psi \leq 35$ deg) as opposed to farther from Sun center ($\psi > 35$ deg), as was done by Eselevich, where each subgroup now numbers either 5 or 6, one still finds no statistically significant preferential association between the parameters. Only one is marginally significant: V_T versus L_f for coincident events that are > 35 deg from Sun center. For that case (6 events),

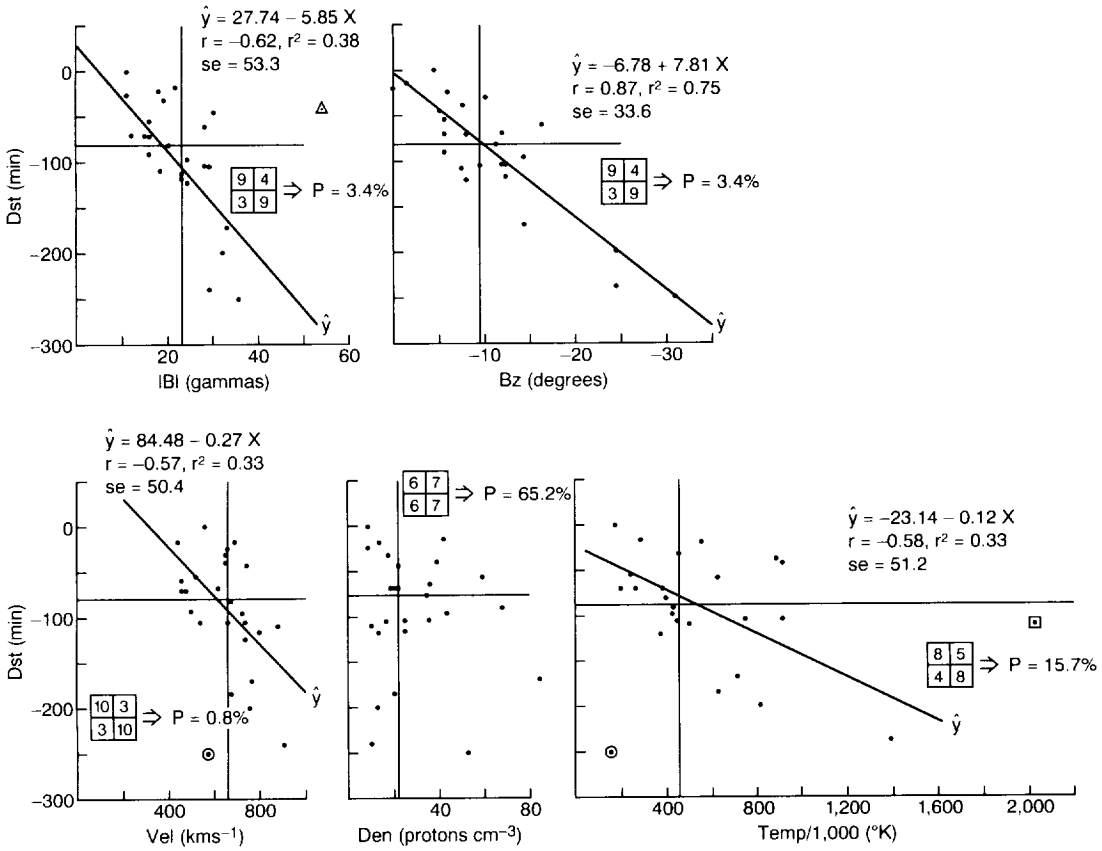

Fig. 7. Scatter plots of Dst(min) versus selected solar wind plasma (velocity, density, and temperature) and field (magnetic field strength and B_z) extremes for the SSC-F events. See text for details

$r = 0.80$, se = 112.3, and the regression equation is $\hat{y} = 521.28 + 5.34x$. It is apparent then that for the SSC-EF events, the average velocity of the associated shock is about $682.9 \pm 44.0\,\mathrm{km\,s^{-1}}$, having an observed range of 390–$1170\,\mathrm{km\,s^{-1}}$ and is independent of filament size and location on the Sun.

Also, recall that Eselevich (1994) has reported that for the SSC-F events, V_T is preferentially associated with J, a characteristic of the X-ray flare, described as the product of the maximum intensity I_m and the square of the time width of the X-ray emission τ^2, and expressed in units of $10^6\,\mathrm{W\,m^{-2}\,h^{-2}}$. The results of the present investigation support his contention. While Eselevich plotted V_T versus J in a linear-log plot, in the present study the plot is linear-linear. The advantage of the linear-linear plot is that it allows the characterization of the inferred relationship to proceed in a more straightforward manner. For example, in Eselevich's paper, the plotted points tend to bunch somewhat closer together at higher J values, and to be spread somewhat farther apart at lower J values. Also, in his analysis, Eselevich ignores several of the events of higher J value for various reasons—the events were considered either too close to the limb or too close in time with other X-ray flares of smaller J value or were characterized as being comprised of several flares whose X-ray bursts merged into one burst of $J > 7$. Excluding these events, he generated a straightline fit that was much steeper than that found in his earlier study (Eselevich, 1990). Ignoring the subset of higher J-valued events (7 of the 9 highest J values) led him to interpret his results in terms of a single grouping of J-valued events, characterizing them instead by their being either coincident or independent of the HCS and being either $> 700\,\mathrm{km\,s^{-1}}$ or not. Unfortunately, his interpretation precluded the much more interesting result of an apparent separation of the V_T versus J correlation into two groupings: a lower J-valued group ($J \leq 56$) in which V_T correlates directly with J and contains both coincident and independent events, with the independent events tending to have higher V_T, and a higher J-valued group ($J > 56$) in which V_T correlates inversely with J, again with independent events tending to be of higher V_T. Such is a result of the present investigation.

The apparent bifurcation of X-ray flares into two J-valued groups, while being unexpected, appears to be true, both empirically and statistically (albeit the small sample size). In particular, intriguing is the rather sharp boundary between low-J valued events and those of high-J value, as well as the form of the correlation within each group: positive or direct correlation for low-J valued events and negative or inverse correlation for high-J valued events. (In Fig. 1, event No. 14 is near the crossover of the two regression lines. In this study, it has arbitrarily been included with the high-J events.)

As a group, low-J events naturally tend to be events of smaller X-ray class (ranging from B3 to X3; see Table 2) and of shorter duration (ranging in length from 7 to 143 min) as compared to high-J events which tend to be of larger X-ray class (ranging from M1 to X15) and of longer duration (ranging in length from 54 to 405 min).

Further, metric type II and/or IV radio emission is less strongly associated with the low-J group as compared to the high-J group, with 7 of 14 low-J events being associated with metric type II and/or IV radio emission as compared to 9 of 12 high-J events being associated with metric type II and/or IV radio emission. Both low- and high-J events tend to be associated with two-ribbon Hα flares (recall the u designation) in equal proportions: exactly 7 of 14 low-J events and 6 of 12 high-J events. Low-J events tend to occur in active regions that are smaller in area and less magnetically complex on the day of the flare than high-J events: 8 of 12 low-J events came from active regions with area $a \leq 445$ millionths of the solar hemisphere as compared to 9 of 12 high-J events that came from regions of $a > 445$ millionths of the solar hemisphere; and 7 of 12 low-J events came from active regions of less magnetic complexity (beta) as compared to 10 of 12 high-J events that came from regions of greater magnetic complexity (i.e. variations of gamma/delta configurations). Thus, the bifurcation of the V_T versus J relationship may be a product of the differences noted here between low- and high-J events and may be indicative of different shock-producing mechanisms in the two groups. Certainly, the latter noted differences between low- and high-J events, regarding area and magnetic complexity of the active region on the day of flaring, suggests a direct link to changes of the magnetic field within the regions (i.e. shear or emerging flux; cf. Zirin, 1990; Feynman and Martin, 1995).

Another interesting aspect of the present study is that 9 out of the 26 SSC-F events were also solar proton events (SPEs) that affected the Earth's environment, with the bulk (6 of 9) being associated with high-J events. Of the high-J events, half (6 of 12) gave rise to SPEs. Figure 8 displays 2×2 contingency tables, comparing J grouping against the various ancillary data listings (recall Table 2). Given is the probability of obtaining the observed result, or one more suggestive of a departure from independence (chance), based upon Fisher's exact test for 2×2 contingency tables. Of the various parameters that might suggest meaningful relationships with J-value, only the duration of the X-ray flare and the area and magnetic complexity of the spot group on the day of flaring seem to be statistically interesting. The X-ray class of the flare is found to be only of marginal statistical significance.

3.2. *Geoeffectiveness*

Concerning the "geoeffectiveness" of the SSC-F events, it was noted that all of the events, except Nos. 17 and 21, had Dst(min)[0–24] several hours after SSC onset, being associated with the solar wind structure behind the shock rather than with the passage of the shock itself. Figure 9 illustrates the behavior of selected solar wind parameters and the behavior of the Dst index during the interval of 24 h before to 36 h following SSC onset for these two events. The parametric behavior of event No. 17 is depicted on the left and of event No. 21 on the right.

Examination of the plasma and field parameters for event No. 17 clearly illustrates that an interplanetary structure swept by Earth following the SSC. The structure was traveling with a speed slightly in excess of the ambient solar wind speed. The structure caused a density enhancement at its leading edge and there was some temperature fluctuation near the leading edge and twice more, each separated by about 10–11 h, although the average temperature was generally low throughout the encounter. A magnetic enhancement began immediately following the shock that remained in excess of 10 gammas for about 24 h. B_z, which had been slightly southward prior to the encounter, abruptly turned strongly northward at 3 h following SSC onset and it remained so throughout the remainder of the encounter, although some evidence for rotation is apparent. Because there was no strong southward component of the interplanetary magnetic field during the passage of the structure associated with event No. 17, no geomagnetic storm should have occurred, and this is evinced from the behavior of Dst during the encounter (see also Table 6). Instead, Dst(min) occurs at SSC onset when B_z was still southward. The observed parametric variations during the passage of the interplanetary structure associated with event No. 17 (a 4B/X3 flare at N35E29) are consistent with the idea that the structure may have been a magnetic cloud that arrived at Earth with northward B_z.

The interplanetary and geomagnetic conditions during the encounter of the structure associated with event No. 21 are much more complex than were seen for event No. 17. For example, the SSC associated with event No. 21 is sandwiched between two other SSCs, one that occurred about 24 h before and another that occurred about 15 h after the one associated with event No. 21. Both the preceding and following SSCs were associated with negative excursions in the Dst index (geomagnetic storms) that were related to the passage of interplanetary magnetic structures at Earth, each having a strong southward B_z. The SSC associated with event No. 21 occurred during the recovery phase of the preceding storm. In terms of the plasma and field parameters, the structure associated with event No. 21 is quite benign, barely attaining a magnetic field strength in excess of 10 gammas and displaying low temperature and northward B_z. Because of the northward B_z, the Dst continued to become more positive in value. Hence, Dst(min) was observed at SSC onset when the Dst index was in recovery phase from a preceding storm rather than later during the event. The behavior that was seen in the encounter of the interplanetary structure associated with event No. 21 (an SF/M1 flare at N09W17), again, is arguably like that which one might expect for a magnetic cloud that arrives at Earth with northward B_z (with the complicating condition that storm recovery is presently underway). (Neither event Nos. 17 or 21 was coincident with the HCS, according to Eselevich (1994).)

Mentioned previously (in connection with Fig. 7; see Section 2.2 was the observation that a few of the events have values of certain solar wind parameters that contrast to the bulk behavior of the events regarding the size of the negative excursion in Dst. These peculiar events include Nos. 5, 9, and 22. Recall that event No. 5 had the highest observed $|B|$ (= 54.4) of the SSC-F events, yet was not particularly geoeffective (Dst(min) = −38). Similarly, while event No. 22 had the highest observed tem-

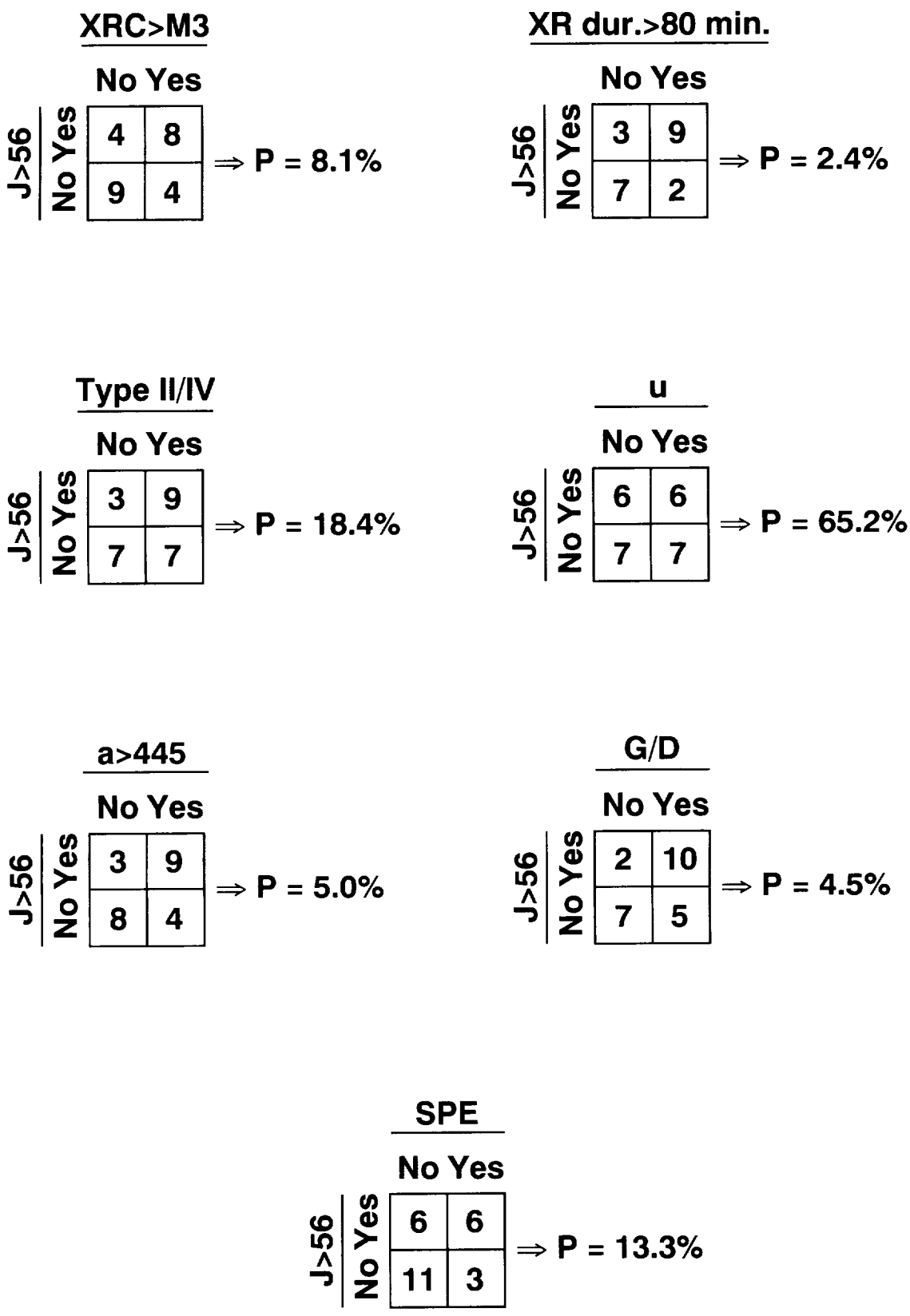

Fig. 8. 2×2 contingency tables for selected pairings of event attributes for SSC-F events (based on *J*). See text for details

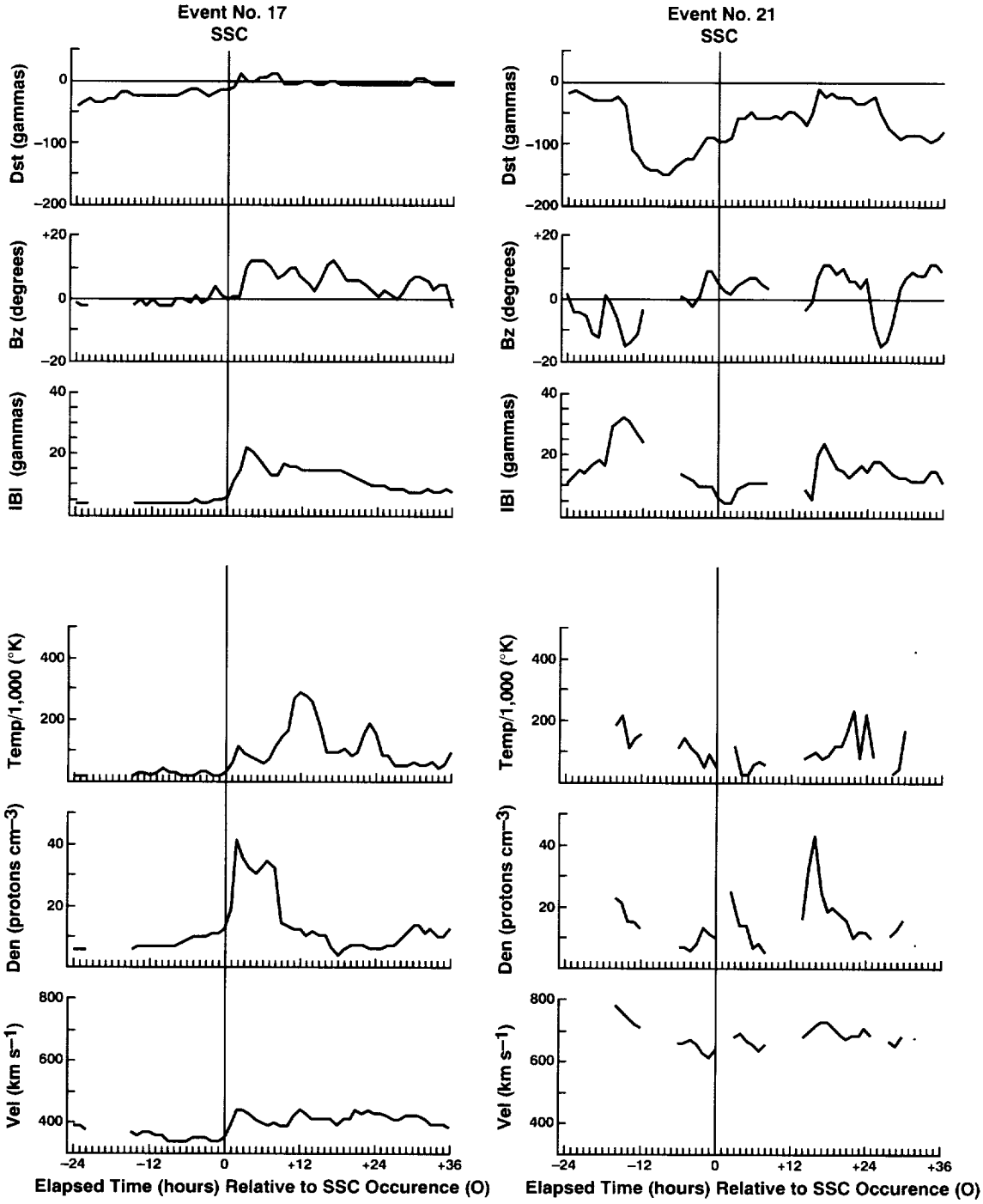

Fig. 9. Solar wind and geomagnetic conditions during the vicinity of SSC-onset for SSC-F event Nos. 17 (left) and 21 (right). See text for details

perature/1000 (= 2119), it was not as geoeffective as one might have expected (Dst(min) = −116). On the other hand, although having the lowest temperature/1000 (164) and not being particularly fast (Vel = 570 km s^{-1}), event No. 9 was the most geoeffective (Dst(min) = −249) of the SSC-F events. Removal of these events from the analyses enhanced the degree of inferred correlation amongst some of the parameters. Figure 10 displays the solar wind and geomagnetic parameters for these peculiar events.

Event No. 5 parameters are displayed in the leftmost panels. A short-lived, possibly rotating, magnetic structure appears to be just ahead of the HCS. Solar wind density, temperature, and magnetic field strength are all observed to quickly lessen in value, beginning about 12 h past SSC onset, while the velocity rises and plateaus at a value of about 600 km s^{-1} and persists so for several days (through June 11). It is speculated that the geoeffectiveness of event No. 5 has been distorted by the presence of the HCS. It should be noted that event No. 5 appears to be related to a bidirectional flow event listed in Gosling *et al.* (1987). Recall that bidirectional flows are thought to be a manifestation of earthward-directed CMEs (as are mag-

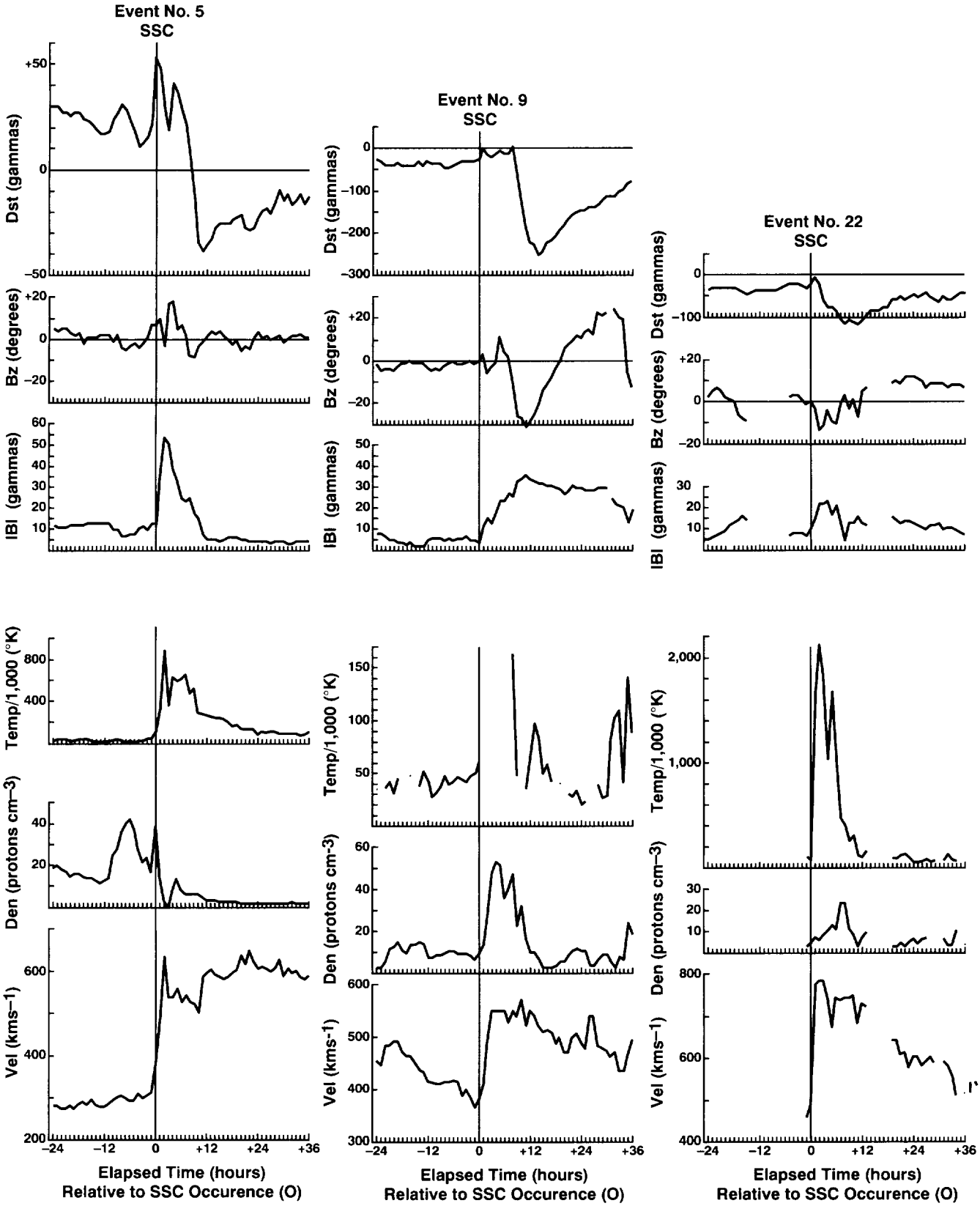

Fig. 10. Solar wind and geomagnetic conditions during the vicinity of SSC-onset for SSC-F event Nos. 5 (left), 9 (center), and 22 (right). See text for details

netic clouds; cf. Klein and Burlaga, 1982; Marsden *et al.*, 1987; Gosling, 1990).

The solar wind and geomagnetic conditions associated with the passage of event No. 9 are displayed in the central panels. Event No. 9 is known to be a magnetic cloud (Zhang and Burlaga, 1988; Wilson, 1990). It was associated with a 2B/M4 flare, located at N06E24 in December 1980. The strongly rotating magnetic fields are plainly associated with the large negative excursion in Dst (strong southward B_z) and the recovery phase of the storm.

The solar wind and geomagnetic conditions associated with the passage of event No. 22 are displayed in the rightmost panels. As with events Nos. 5 and 9 (and others), it too seems to be suggestive of a rotating, magnetic structure that passes Earth. Like event No. 9, it occurs independent of the HCS (according to Eselevich (1994)).

Two other events that are known to be associated with earthward-directed CMEs include events Nos. 1 and 3. Both events are listed in tables of bidirectional flow events (Gosling *et al.*, 1987; Marsden *et al.*, 1987) and event No. 1 is also listed as a magnetic cloud (Zhang and Burlaga, 1988; Wilson, 1990). Figure 11 depicts the solar wind and geomagnetic conditions associated with these events. Event No. 1 is shown on the left and event No. 3 on the right. Event No. 1 has the second largest negative Dst excursion ($= -241$) of the SSC-F events and like event No. 9 is a low-J event.

Figure 12 displays the results of superposed epoch analyses of the SSC-F events, subdividing the events into two categories: those that were found to be geoeffective (comprised of the 14 events that had Dst(min) ≤ -75 and depicted using the heavy line in all panels) and those that were not (comprised of 12 events and depicted using the thin line in all panels). Shown are the solar wind and geomagnetic conditions in the vicinity of SSC onset (24 h prior to SSC onset to 36 h after SSC onset). One finds that geoeffective SSC-F events are characterized (on average) as events of higher solar wind speed, both before SSC onset (ambient conditions) and following SSC onset, and greater magnetic field strength as compared to SSC-F events that were not associated with a Dst(min) ≤ -75. They also had a stronger southward component of the interplanetary magnetic field. For the geoeffective events, one observes that $<$Dst$>$ becomes more negative in value precisely when $<B_z>$ turns southward and recovery does not begin until the B_z component has returned to smaller southward values (or has become northward). While nongeoeffective SSC-F events (on average) are slower and less intense magnetically than geoeffective SSC-F events and while they tend to have more northerly B_z, one finds that their $<$Dst$>$ behaves somewhat similarly to that found for geoeffective SSC-F events, albeit on a smaller scale. For example, $<$Dst$>$ decreases from a pre-SSC onset average of about -13 to -27, attaining minimum value several hours following SSC onset, for the nongeoeffective events; for the geoeffective events, $<$Dst$>$ decreases from about -48 to -78 over a similar time frame. In the statistical sense, the observed signatures are statistically important and the differences between geoeffective and nongeoeffective events are statistically significant, with the lone exception being the pre-SSC onset averages of the magnetic field strengths. The slightly enhanced $<$Den$>$ and $<$Temp/1000$>$ for the pre-SSC onset interval of the geoeffective events are attributed to their larger $<$Vel$>$.

It would be most satisfying if one could know ahead of time the identity of those SSC-F events (all with $J \geq 7$, a ranking found by Eselevich (1990) to be indicative of events that can give rise to SSCs) that will most likely generate geomagnetic storms. Unfortunately, there is no one-to-one descriptor that is presently known that can do this. Based on J, it was shown that high-J events tend to be associated with Ap(max) ≥ 30 (9 of 12 events; recall Fig. 3). However, in general, Ap(max) ≥ 30 associates equally with both low-J and high-J events. In terms of Dst(min), the association between Dst(min) ≤ -75 occurrences and high-J events is weaker with only 7 of 12 high-J events being termed "geoeffective" and with all geoeffective SSC-F events being equally split between events of high-J and low-J value (see Fig. 5). So, while the value of J may give a better estimate for the timing of SSC onset (from Fig. 1), it alone says little about what to expect geomagnetically. From Fig. 12, it was shown that geoeffective SSC-F events tend to be associated with solar wind flows that are of high $<$Vel$>$, enhanced $<|B|>$, and strong southward magnetic field. Of these parameters, only $<$Vel$>$ might be crudely estimated beforehand. For example, one expects $<$Vel$>$ to be associated with V_T. Using the J-value as a predictor, one can estimate V_T which in turn can be used to estimate $<$Vel$>$. If the resultant $<$Vel$>$ exceeds a certain value, then one might venture to predict that a geomagnetic storm should follow the expected SSC.

Figure 13 plots the average velocity of the solar wind during the first 36 h following SSC onset (dubbed $<$Vel$>$[1–36]) against the inferred transit velocity of the shock V_T, as deduced by Eselevich (1994), for the 26 SSC-F events. Filled circles denote the 14 geoeffective events and unfilled circles the 12 nongeoeffective events, where a geoeffective event is one that has Dst(min) ≤ -75. The median V_T is noted (by the vertical line) to be about 920 km s^{-1} and the median $<$Vel$>$[1–36] (by the horizontal line) to be about 590 km s^{-1}. Specific events are numbered. Based on the 2×2 contingency table (lower right), one finds that 9 of 14 SSC-F events with $V_T \geq 920$ km s^{-1} are geoeffective; similarly, 7 of 12 SSC-F events with $V_T < 920$ km s^{-1} are nongeoeffective. Therefore, given V_T, one possibly could have correctly predicted the occurrence or lack of occurrence of a geomagnetic storm for 16 of the 26 SSC-F events (a skill level of about 62%). Unfortunately, the two largest storms (based on Dst(min)) associated with events Nos. 1 and 9 would have been incorrectly predicted. (A linear regression fit is also displayed in Fig. 13, one that, while being statistically important, can explain only 28% of the variance in $<$Vel$>$[1–36]. Also, one should note that $<$Vel$>$[1–36] exceeds V_T for events Nos. 12 and 20, perhaps, suggesting the possibility of an error in V_T for these events. Both events were coincident with the HCS, according to Eselevich (1994).)

A comparison of the occurrence or lack of occurrence of specific observable parameters associated with each flare against the geoeffectiveness of the events is shown in Fig. 14. Of all the parameters listed in Table 2, only five appear possibly useful for prediction purposes. These

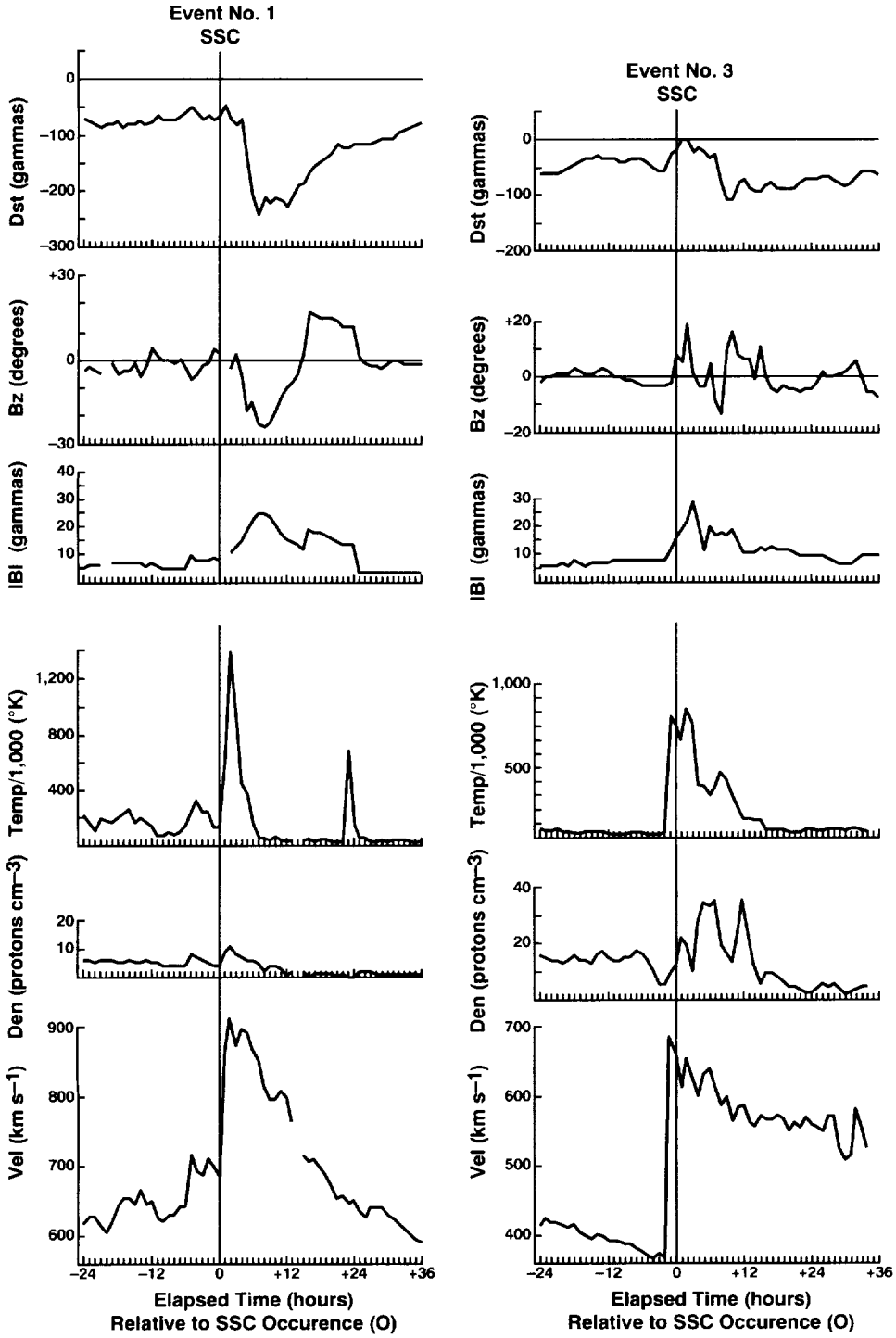

Fig. 11. Solar wind and geomagnetic conditions during the vicinity of SSC-onset for SSC-F event Nos. 1 (left) and 3 (right). See text for details

include, in reverse order of importance (from least to most), the Hα flare importance (IMP), the areal size of the active region (*a*), the duration of the X-ray event (XR dur.), the appearance of a two-ribbon flare structure (*u*), and the hemisphere in which the flare occurred (eastern). For example, 6 of 25 SSC-F events of known Hα optical importance were associated with either subflares or flares of IMP 1. Of these 6 nonmajor flares, 5 were geoeffective. The inference, then, is that if an Hα flare occurs and it can be associated with an X-ray flare that has a *J* characteristic ≥ 7, one might expect it to be highly likely of generating a geomagnetic storm. On the other hand, if the flare was ranked as a major flare (IMP ≥ 2), then one expects the flare to have about a 50–50 chance of generating a storm

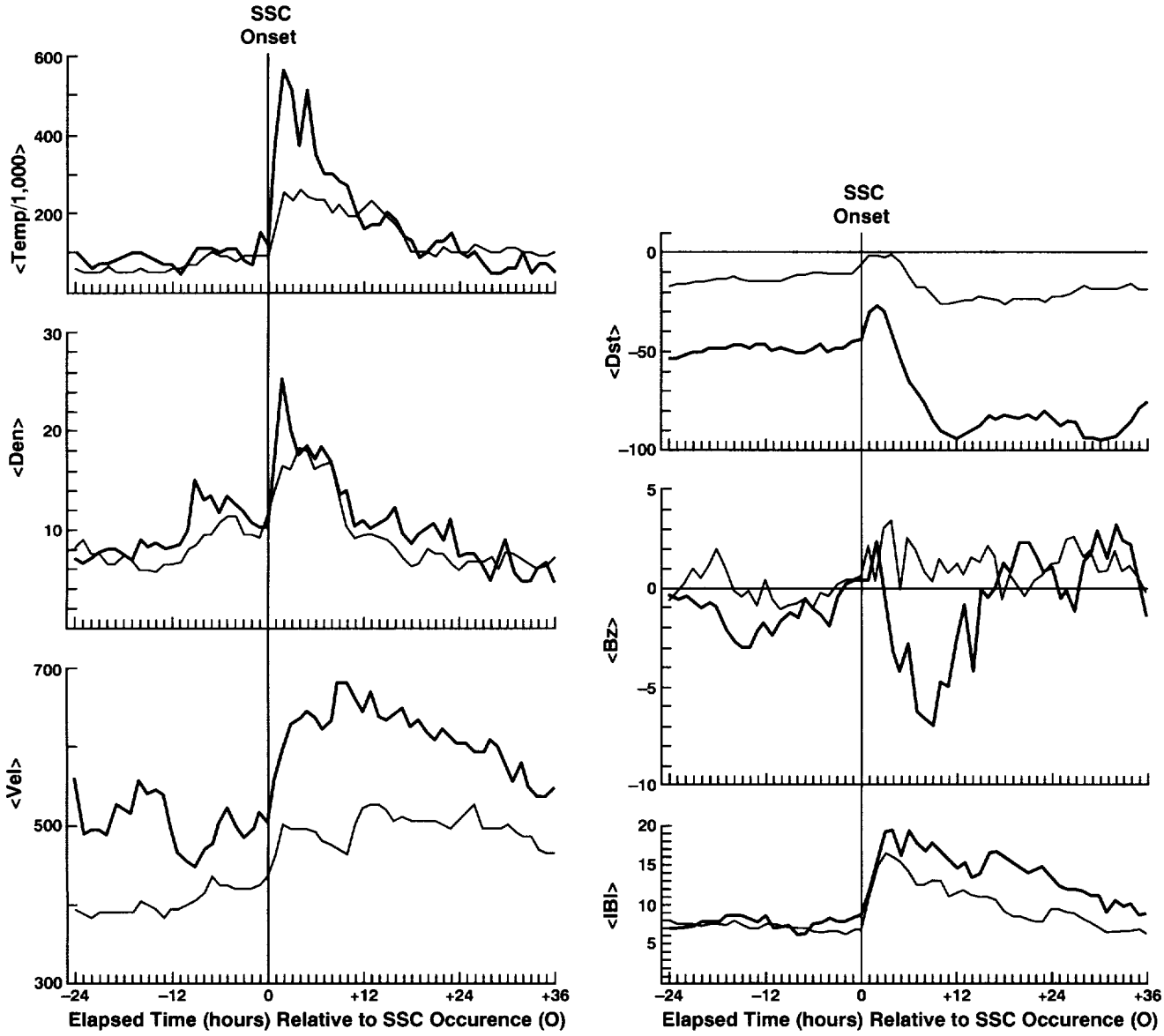

Fig. 12. Solar wind and geomagnetic conditions during the vicinity of SSC-onset for SSC-F events based on a superposed epoch analysis. The heavy line denotes those SSC-F events that were found to be geoeffective and the thin line those that were found to be nongeoeffective. See text for details

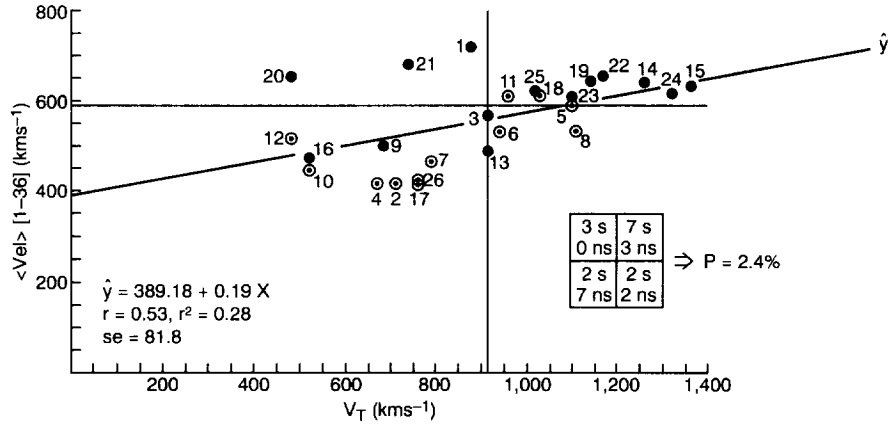

Fig. 13. Scatter plot of the average velocity of the solar wind during the first 36 h following SSC-onset <Vel> [1–36] versus V_T. Filled circles denote those SSC-F events that were geoeffective (storm s) and unfilled circles those that were found to be nongeoeffective (no storm ns). See text for details

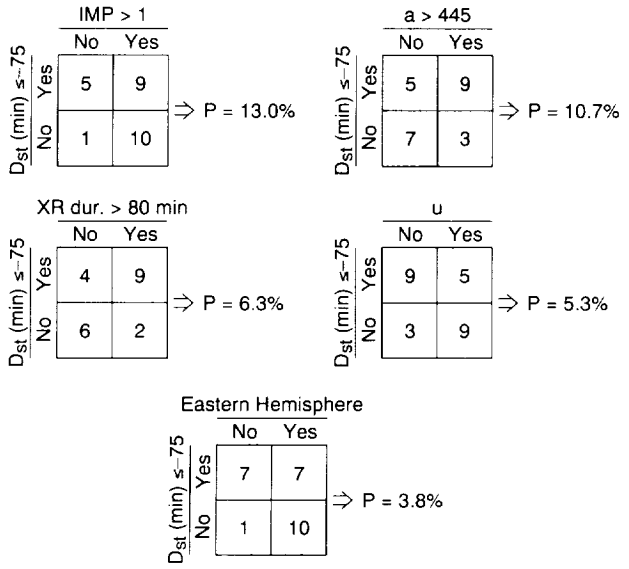

Fig. 14. 2×2 contingency tables for selected pairings of event attributes for SSC-F events (based on Dst(min)). See text for details

(only 9 of 19 could be associated with Dst(min) ≤ -75).

Continuing, of the 24 SSC-F events of known areal extent, 12 occurred in active regions of $a > 445$ millionths of a solar hemisphere and, of these, 9 were geoeffective. Of the 12 that had $a \leq 445$, 7 were nongeoeffective. Thus, given a flare of $J \geq 7$ and the areal extent of the region from which the flare emanated, one might have been able to correctly predict the occurrence or lack of occurrence of a storm in 16 of 24 events (67%). Following this approach, one would have predicted event No. 9 to be geoeffective, but not event No. 1.

Because sometimes a small flare can be associated with $J \geq 7$, an important parameter regarding its ability to generate a storm should be the duration of the X-ray event. Indeed, Fig. 14 illustrates that of the 21 SSC-F events for which the X-ray duration is known, 11 were of long duration (>80 min). Of these, 9 were geoeffective. Of the 10 SSC-F events of XR duration ≤ 80 min, 6 were nongeoeffective. Thus, given a flare of $J \geq 7$ and the X-ray duration of the flare, one might have been able to correctly predict the occurrence or lack of occurrence of a storm in 15 of 21 events (71%).

Surprisingly, one finds that the *lack* of appearance of a two-ribbon flare structure (u) is a better predictor for geoeffectiveness than having it. Of the 26 SSC-F events, 14 had the two-ribbon flare structure. Of these, 9 were nongeoeffective. Of the 12 that did not have the two-ribbon flare structure, 9 were geoeffective. Thus, given a flare of $J \geq 7$ and the appearance or lack of appearance of two-ribbon flare structure, one might have been able to correctly predict the occurrence or lack of occurrence of a storm in 18 of 26 events (69%).

Finally, of the 25 SSC-F events that occurred with known hemispheric location, 17 occurred in the eastern hemisphere and 8 in the western hemisphere. Of the 17 eastern hemispheric events, 10 were nongeoeffective; of the 8 western hemispheric events, 7 were geoeffective. Thus, given a flare of $J \geq 7$ and knowledge of its location, one might have been able to correctly predict the occurrence or lack of occurrence of a storm in 17 of 25 events (68%).

Using only the latter two parameters (hemispheric location and two-ribbon structure) in conjunction with the X-ray characteristic ($J \geq 7$) for a determination of geoeffectiveness (ignoring event No. 10 because its location and Hα importance are unknown; see Table 2), one finds that if either the event occurred in the western hemisphere or lacked a two-ribbon structure and the characteristic X-ray parameter $J \geq 7$, then the event usually was geoeffective (true for 12 of 15 events) and, conversely, if the event both occurred in the eastern hemisphere and had a two-ribbon flare structure and it had $J \geq 7$, then the event usually was nongeoeffective (true for 8 of 10 events). Thus, given a flare of $J \geq 7$ and knowledge of both its location and appearance or lack of appearance of two-ribbon structure, one might have been able to correctly predict the occurrence or lack of occurrence of a storm in 20 of 25 events (80%). In the foregoing example, events Nos. 20 and 24 would have been incorrectly predicted to be nongeoeffective (in actuality, they were the fifth and third largest negative excursion events, respectively) and events Nos. 6, 8, and 11 would have been incorrectly predicted to be geoeffective. Of these five events, only event No. 20 was coincident with the HCS (according to Eselevich (1994)). All of the events were major flares and all were events of high-J value, except events Nos. 11 ($J = 53$) and 20 ($J = 18$). (See Table 2 for a detailed comparison of observables.)

Figure 15 displays the solar wind and geomagnetic conditions in the vicinity of SSC onset for these five peculiar events. Events Nos. 6, 8, and 11 (nongeoeffective events) are depicted in the leftmost panels, while events Nos. 20 and 24 (geoeffective events) are depicted in the rightmost panels. Although the solar wind data are incomplete for some of the events, plainly, the nongeoeffective events were slower and of less magnetic field strength than the geoeffective events. Likewise, the B_z component tended to be pointed in the northerly direction and lacked a strong southward rotation, whereas the geoeffective events tended to be pointed in the southerly direction just following SSC onset and showed a strong southward (and northward) rotation, indicative of magnetic cloud/bidirectional flow events. Based on the observables for these events (Table 2), in conjunction with the proposed scheme for determining geoeffectiveness of $J \geq 7$ events, one must recognize that the strongest indicator for geoeffectiveness is the strength of the southward magnetic field following SSC onset at Earth; hence, one will not be able to correctly predict the geoeffectiveness of these events (with 100% certainty) until one can correctly model the behavior of the structure's internal magnetic field during Earth passage.

4. Conclusions

The major results of the present study are summarized below:

No preferential relationship is found to exist between the size of the eruptive filament L_f and the transit speed

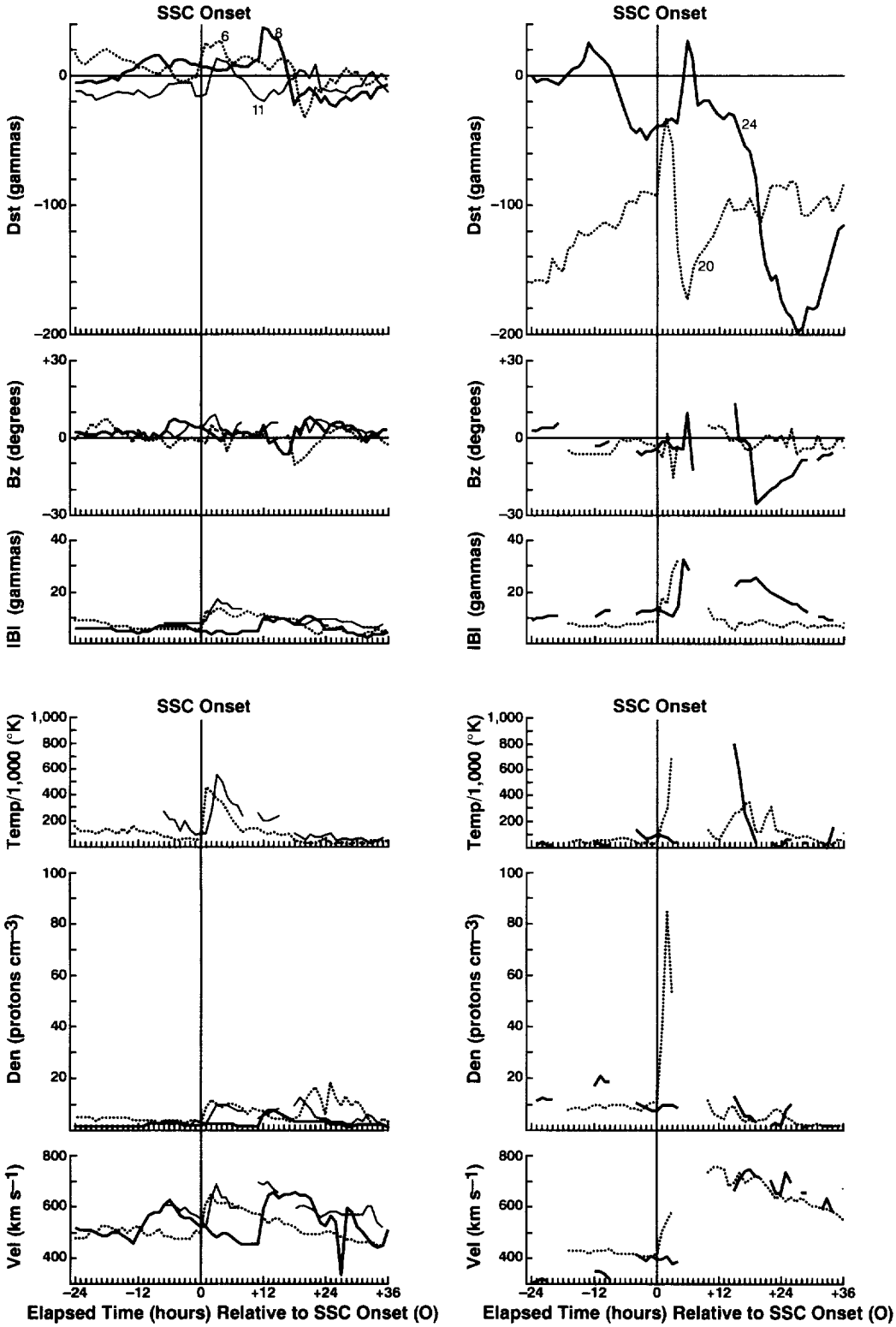

Fig. 15. Solar wind and geomagnetic conditions during the vicinity of SSC-onset for SSC-F event Nos. 6, 8, and 11 (left—nongeoeffective events) and 20 and 24 (right—geoeffective events). See text for details

of the shock V_T for the 21 SSC-EF events identified by Eselevich (1994). This is true even when one uses smaller subsets (e.g. purely coincident events that are located >35 deg from the center of the Sun). Thus, this finding refutes the claim by Eselevich that such a relationship exists.

A preferential relationship is found to exist between the value of the X-ray characteristic J and V_T for the 26 SSC-

F events identified by Eselevich (1994). While this finding supports the view of Eselevich that such a relationship exists, the present study demonstrates that the relationship is possibly more complicated than originally thought. It appears that the set of SSC-F events can be subdivided into two groups: a low-J group ($J \leq 56$) and a high-J group ($J > 56$). For both groups, a preferential relationship exists between V_T and J, however, dependent upon grouping, the relationship is either direct (low-J) or inverse (high-J).

As a whole, V_T for the SSC-F events tends to be larger than for the SSC-EF events, and V_T for shocks that arrive independently of the HCS tends to be larger than those that arrive coincidently with the HCS (for the SSC-F events only). Further, high-J events tend to have larger V_T than low-J events.

In contrast to low-J events, high-J events tend to be associated with flares of greater XRC and longer duration, to occur in active regions that are large in areal extent and magnetically complex (gamma/delta), and to be more strongly associated with the occurrences of metric type II/IV radio emission.

Of nine solar proton events that affected the Earth's environment that were associated with SSC-F events, six were high-J events.

Of the 26 SSC-F events, 14 could be described as being "geoeffective" (i.e. associated with geomagnetic storms that had Dst(min) ≤ -75). Those SSC-F events that were found to be geoeffective appear to be faster and of greater inherent magnetic field strength than those that were not considered to be geoeffective.

The degree of geoeffectiveness was directly related to the strength of the southward magnetic field B_z.

Several of the SSC-F events are noted to also be described as "magnetic clouds" and/or "bidirectional flow events", thus supporting the view that the SSC-F events are probably fast earthward-directed CMEs.

No preferential relationship was found between J and the degree of geoeffectiveness for the SSC-F events.

A simple paradigm for determining the likelihood that an SSC-F event will or will not be geoeffective was found, based on Eselevich's SSC-F events; namely, if a solar flare occurs that has a computed $J \geq 7$ and it either occurs in the western hemisphere or does not have a two-ribbon flare structure, one expects the event to be geoeffective, while if the event both occurs in the eastern hemisphere and has a two-ribbon flare structure, one expects the event to be nongeoeffective. Such a scheme was found to have correctly postdicted the occurrence or lack of occurrence of storms for the SSC-F events at a skill level of 80%.

Acknowledgements. The author thanks Steven T. Suess (NASA Marshall Space Flight Center, Huntsville, Alabama) for reading both the original and revised manuscripts and the unnamed referees who provided the impetus to provide a more extensive examination of Eselevich's events, especially with regard to the question of geoeffectiveness.

References

Akasofu, S. I. and Chapman, S., *Solar-Terrestrial Physics.* Oxford University Press, London, 1972.

Cane, H. V., The evolution of interplanetary shocks. *J. Geophys. Res.* **90**(A1), 191–197, 1985.

Cane, H. V., Kahler, S. W. and Sheeley Jr, N. R., Interplanetary shocks preceded by solar filament eruptions. *J. Geophys. Res.* **91**(A12), 13,321–13,329, 1986a.

Cane, H. V., McGuire, R. E. and Rosenvinge, T. T. von, Two classes of solar energetic particle events associated with impulsive and long-duration soft X-ray flares. *Astrophys. J.* **301**, 448–459, 1986b.

Chao, J. K. and Lepping, R. P., A correlative study of ssc's, interplanetary shocks, and solar activity. *J. Geophys. Res.* **79**(A13), 1799–1807, 1974.

Cliver, E. W., Solar activity and geomagnetic storms: from M regions and flares to coronal holes and CMEs. *Eos, Trans. Am. Geophys. Un.* **76**(8), 75, 83, 1995a.

Cliver, E. W., Solar flare nomenclature. *Solar Phys.* **157**, 285–293, 1995b.

Couzens, D. A. and King, J. H., *Interplanetary Medium Data Book – Supplement 3A*, 1977–1985, NSSDC/WDC-A-R&S 86-04a. NASA/GSFC, Greenbelt, Maryland, April 1986.

Ehrenberg, A. S. C., *A Primer in Data Reduction.* Wiley, New York, 1982.

Eselevich, V. G., Solar flares: geoeffectiveness and the possibility of a new classification. *Planet. Space Sci.* **38**(2), 189–206, 1990.

Eselevich, V. G., Quantitative characteristics of solar active process and their relationship with the transit velocity of interplanetary shock waves. *Planet. Space Sci.* **42**(7), 575–582, 1994.

Eselevich, V. G., Fainshtein, V. G. and Filippov, M. A., On the problem of geoeffectiveness of sporadic phenomena on the Sun. *Planet. Space Sci.* **36**(10), 1015–1023, 1988.

Everitt, B. S., *The Analysis of Contingency Tables.* Wiley, New York, 1977.

Feynman, J. and Hundhausen, A. J., Coronal mass ejections and major flares: the great active center of March 1989. *J. Geophys. Res.* **99**(A5), 8451–8464, 1994.

Feynman, J. and Martin, S. F., The initiation of coronal mass ejections by newly emerging magnetic flux. *J. Geophys. Res.* **100**(A3), 3355–3367, 1995.

Gosling, J. T., Coronal mass ejections and magnetic flux ropes in interplanetary space, in *Physics of Magnetic Flux Ropes* (edited by C. T. Russell, E. R. Priest and L. C. Lee), Geophysical Monograph 58, pp. 343–364. AGU, Washington, DC, 1990.

Gosling, J. T., The solar flare myth. *J. Geophys. Res.* **98**(A11), 18,937–18,949, 1993.

Gosling, J. T., Reply. *J. Geophys. Res.* **100**(A3), 3479–3480, 1995a.

Gosling, J. T., Reply. *J. Geophys. Res.* **100**(A5), 7921–7923, 1995b.

Gosling, J. T., Baker, D. N., Bame, S. J., Feldman, W. C. and Zwickl, R. D., Bidirectional solar wind electron heat flux events. *J. Geophys. Res.* **92**(A8), 8519–8535, 1987.

Gosling, J. T., Bame, S. J., McComas, D. J. and Phillips, J. L., Coronal mass ejections and large geomagnetic storms. *Geophys. Res. Lett.* **17**(7), 901–904, 1990.

Gosling, J. T., McComas, D. J., Phillips, J. L. and Bame, S. J., Geomagnetic activity associated with Earth passage of interplanetary shock disturbances and coronal mass ejections. *J. Geophys. Res.* **96**(A5), 7831–7839, 1991.

Harrison, R. A., Coronal transients and their relation to solar flares. *Adv. Space Res.* **11**(1), 25–36, 1991.

Harrison, R. A. and Sime, D. G., The launch of coronal mass ejections: white light and X-ray observations in the low corona. *J. Geophys. Res.* **94**(A3), 2333–2344, 1989.

Hudson, H., Haisch, B. and Strong, K. T., Comment on "The solar flare myth" by J. T. Gosling. *J. Geophys. Res.* **100**(A3), 3473–3477, 1995.

Hundhausen, A. J., The origin and propagation of coronal mass

ejections, in *Proceedings of the Sixth International Solar Wind Conference* (edited by V. J. Pizzo, T. Holzer and D. G. Sime), NCAR/TN-306+Proc (Technical Note), Vol. 1, pp. 181–214. NCAR/HAO, Boulder, Colorado, May 1988.

Joselyn, J. A., Geomagnetic activity forecasting: the state of the art. *Rev. Geophys.* **33**(3), 383–401, 1995.

Kahler, S. W., Solar flares and coronal mass ejections. *Ann. Rev. Astron. Astrophys.* **30,** 113–141, 1992.

Kahler, S. W., Sheeley Jr, N. R., Howard, R. A., Koomen, M. J., Michels, D. J., McGuire, R. E., Rosenvinge, T. T. von and Reames, D. V., Associations between coronal mass ejections and solar energetic proton events. *J. Geophys. Res.* **89**(A11), 9683–9693, 1984.

Kahler, S. W., Sheeley Jr, N. R. and Liggett, M., Coronal mass ejections and associated X-ray flare durations. *Astrophys. J.* **344,** 1026–1033, 1989.

King, J. H., *Interplanetary Medium Data Book—Supplement* 4, 1985–1988, NSSDC/WDC-A-R and S 89-17. NASA/GSFC, Greenbelt, Maryland, September 1989.

King, J. H. and Papitashvili, N. E., *Interplanetary Medium Data Book—Supplement* 5, 1988–1993, NSSDC/WDC-A-R and S 94-08. NASA/GSFC, Greenbelt, Maryland, September 1994.

Klein, L. W. and Burlaga, L. F., Interplanetary magnetic clouds at 1 AU. *J. Geophys. Res.* **87**(A2), 613–624, 1982.

Lapin, L. L., *Statistics for Modern Business Decisions*, 2nd Edn. Harcourt Brace Jovanovich, New York, 1978.

Marsden, R. G., Sanderson, T. R., Tranquille, C. and Wenzel, K.-P., ISEE 3 observations of low-energy proton bidirectional events and their relation to isolated interplanetary magnetic structures. *J. Geophys. Res.* **92**(A10), 11,009–11,019, 1987.

Mendoza, B. and Perez-Enriquez, R., Association of coronal mass ejections with the heliomagnetic current sheet. *J. Geophys. Res.* **98**(A6), 9365–9370, 1993.

Mendoza, B. and Perez-Enriquez, R., Geoeffectiveness of the heliospheric current sheet. *J. Geophys. Res.* **100**(A5), 7877–7880, 1995.

Nonnast, J. H., Armstrong, T. P. and Kohl, J. W., A study of solar flare soft X rays and their relation to particle events observed by IMP 8. *J. Geophys. Res.* **87**(A6), 4327–4337, 1982.

Patel, V. L., 14. Solar-terrestrial physics, in *Illustrated Glossary for Solar and Solar-Terrestrial Physics* (edited by A. Bruzek and C. J. Durrant), Astrophysics and Space Science Library, Vol. 69, pp. 159–193. D. Reidel, Dordrecht, Holland, 1977.

Pudovkin, M. I., Comment on "The solar flare myth" by J. T. Gosling. *J. Geophys. Res.* **100**(A5), 7917–7919, 1995.

Richardson, I. G., A survey of bidirectional >1 MeV ion flows during the Helios 1 and Helios 2 missions: observations from the Goddard Space Flight Center instruments. *Astrophys. J.* **420,** 926–942, 1994.

Sheeley Jr, N. R., Howard, R. A., Koomen, M. J., Michels, D. J., Schwenn, R., Muhlhauser, K. H. and Rosenbauer, H., Coronal mass ejections and interplanetary shocks. *J. Geophys. Res.* **90**(A1), 163–175, 1985.

Tang, F., Tsurutani, B. T., Gonzalez, W. D., Akasofu, S. I. and Smith, E. J., Solar sources of interplanetary southward B_z events responsible for major magnetic storms (1978–1979). *J. Geophys. Res.* **94**(A4), 3535–3541, 1989.

Webb, D. F. and Hundhausen, A. J., Activity associated with the solar origin of coronal mass ejections. *Solar Phys.* **108,** 383–401, 1987.

Webb, D. F., Forbes, T. G., Aurass, H., Chen, J., Martens, P., Rompolt, B., Rusin, V. and Martin, S. F., Material ejection. *Solar Phys.* **153,** 73–89, 1994.

Wilson, R. M., Geomagnetic response to magnetic clouds. *Planet. Space Sci.* **35**(3), 329–335, 1987.

Wilson, R. M., Reply. *Planet. Space Sci.* **36**(12), 1489–1493, 1988.

Wilson, R. M., On the behavior of the Dst geomagnetic index in the vicinity of magnetic cloud passages at Earth. *J. Geophys. Res.* **95**(A1), 215–219, 1990.

Zhang, G. and Burlaga, L. F., Magnetic clouds, geomagnetic disturbances, and cosmic ray decreases. *J. Geophys. Res.* **93**(A4), 2511–2518, 1988.

Zirin, H., Solar flares, in *Physics of Magnetic Flux Ropes* (edited by C. T. Russell, E. R. Priest and L. C. Lee), Geophysical Monograph 58, pp. 33–42. AGU, Washington, DC, 1990.